Palaeogeography, Palaeoclimatology, Palaeoecology 543 (2020) 109565

Contents lists available at ScienceDirect

Palaeogeography, Palaeoclimatology, Palaeoecology

journal homepage: www.elsevier.com/locate/palaeo

Paleoproduction and environmental change at Mono Lake (eastern Sierra Nevada) during the Pleistocene-Holocene transition

Bailee N. Hodelka[a], Michael M. McGlue[a,*], Susan Zimmerman[b], Guleed Ali[c,d], Irene Tunno[b]

[a] Department of Earth and Environmental Sciences, University of Kentucky, Lexington, KY, USA
[b] Center for Accelerator Mass Spectrometry, Lawrence Livermore National Laboratory, Livermore, CA, USA
[c] Climate Change Institute, University of Maine, Orono, ME, USA
[d] Earth Observatory of Singapore, Singapore

ARTICLE INFO

Keywords:
California
Lithostratigraphy
Paleoshorelines
Paleolimnology
Radiocarbon

ABSTRACT

The late Quaternary limnological history of Mono Lake (~16.6–4.3 cal kyr BP), a hydrologically closed basin in the eastern Sierra Nevada (California), is inferred based on a multi-indicator analysis of a long (~10.8 m) composite sediment core constructed from overlapping deepwater piston cores. The composite core, dated by ^{14}C and tephra correlation, shows variations in sedimentology, magnetic susceptibility, elemental geochemistry and stable isotopes through time, consistent with changes in aquatic productivity, hydroclimate, and volcanism. In the late Pleistocene, deepwater stratigraphy was influenced by high-amplitude water-level changes and runoff from a glaciated watershed. In contrast, Mono Lake's elevation was lower in the Early to Middle Holocene; low-amplitude water-level changes, wave reworking of the shoreline, and water-column stratification were important controls on facies during that time. The data suggest that the chief controls on organic facies development in Mono Lake – productivity, preservation, and dilution dynamics – are sensitive to climate changes that influence lake-level elevation, water chemistry, and the position of deltas. The study shows that deepwater sediments from certain locales in Mono Lake are well-preserved, continuous, and can be reliably dated with ^{14}C applied to terrestrial materials. When paired with precisely dated paleoshoreline data, these sediments provide a high-resolution archive of deglacial and Holocene environmental information for the eastern Sierra Nevada.

1. Introduction

The Sierra Nevada forms the headwaters for much of California, as seasonal snowmelt from these mountains provides the USA's largest population and economy with freshwater (Hayhoe et al., 2004; Viers and Rheinheimer, 2011). As a consequence, the impacts of environmental change on California's hydroclimate in general and the Sierran snowpack in particular remain topics of great interest (e.g., Mauer, 2007; MacDonald et al., 2008; Griffin and Anchukaitis, 2014; Diffenbaugh et al., 2015). Mono Lake is a hydrologically closed lake located in the rain shadow of the Sierra Nevada in northeastern California (Fig. 1). The lake's hydrology is strongly influenced by the same Pacific Ocean moisture sources that affect the Sierras (Stine, 1987; Benson et al., 2003a; Zimmerman et al., 2011a). Hydrologically closed lakes are well-known for their sensitivity to climate change; sediments and fossils from endorheic basins provide important paleoenvironmental insights for many arid regions globally (e.g., Laird et al., 1996; Oviatt, 1997; Lowenstein et al., 1999; Colman et al., 2007; McGlue et al., 2017). Thus, Mono Lake sediments hold great promise as archives for understanding the environmental history of the Sierra Nevada.

Outcrops of lacustrine silts and tephras deposited in Late Pleistocene Mono Lake have been studied extensively (Lajoie, 1968; Newton, 1994; Benson et al., 1998; Zimmerman et al., 2011a, 2011b). These sediments, known as the Wilson Creek Formation (WCF), represent deposition from ~67 to 12 kyr B.P. (Zimmerman et al., 2006). Lajoie (1968) was the first to examine the WCF in detail. The stratigraphy of the WCF suggests that Mono Lake did not overflow during the last glacial cycle, which means that paleoshoreline elevations most likely reflect the balance between precipitation and evaporation during that period (Zimmerman et al., 2011a). The prominent paleoshorelines surrounding Mono Lake therefore provide a record of the response of water level and volume to these climatic parameters. More recently, Ali (2018) developed a Mono Lake paleoshoreline chronology for the late Pleistocene, and suggested that several high amplitude water level changes occurred from ~25.0–12.0 kyr B.P. Geomorphological and stratigraphic data presented by Stine (1990) for the past four millennia

* Corresponding author at: Department of Earth and Environmental Sciences, University of Kentucky, 121 Washington Ave, Lexington, KY 40506, USA.
E-mail address: michael.mcglue@uky.edu (M.M. McGlue).

https://doi.org/10.1016/j.palaeo.2019.109565
Received 14 August 2019; Received in revised form 19 December 2019; Accepted 23 December 2019
Available online 02 January 2020

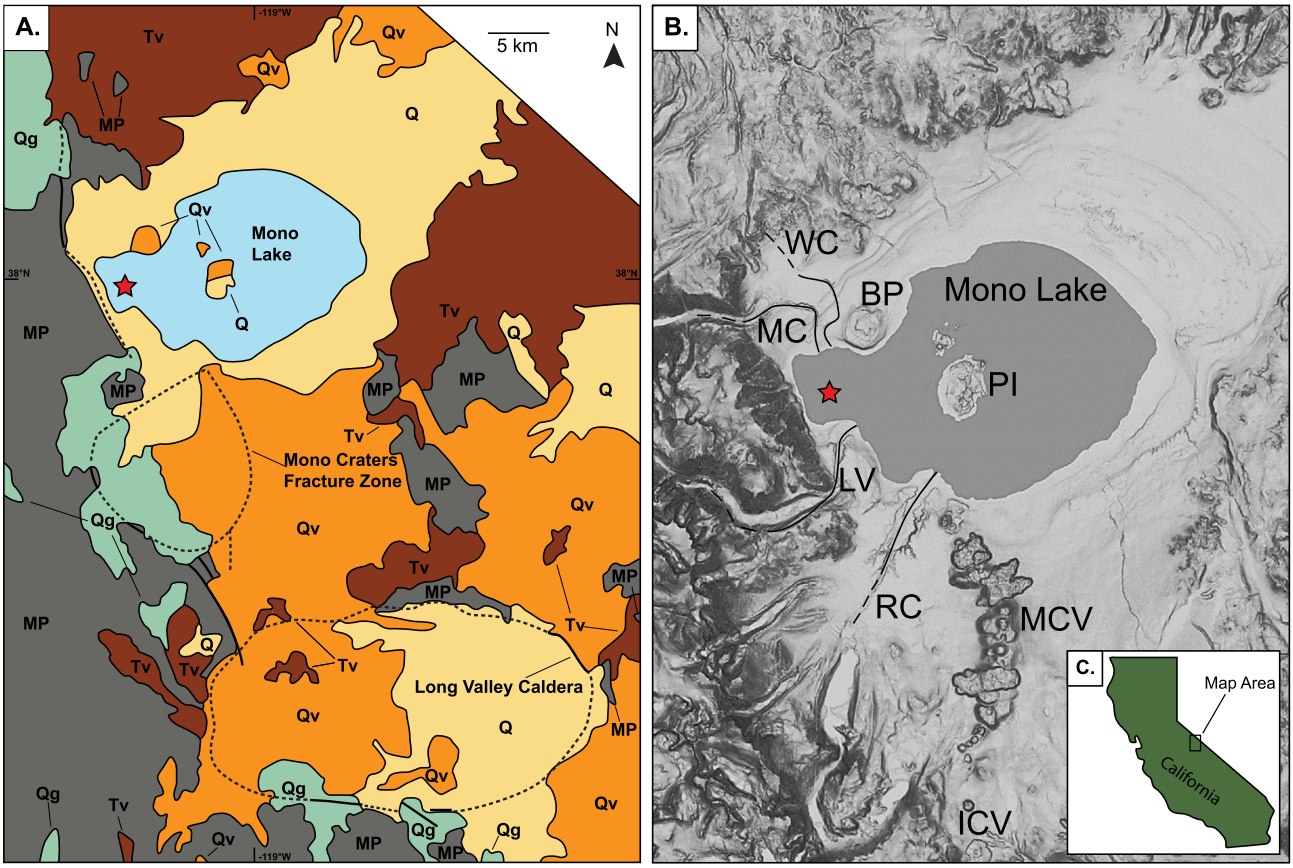

Fig. 1. (A) Generalized geologic map of Mono Lake (modified from Jennings et al., 2010). Q, Quaternary (general). Qg, Quaternary glacial deposits. Qv, Quaternary volcanic deposits. Tv, Tertiary volcanic deposits. MP, Mesozoic and Paleozoic sedimentary, metasedimentary, and igneous rocks. (B) Digital elevation model of the study area. Stars mark the coring location. (C) Location of map of the study site in California.

provide strong evidence for six transgressive-regressive cycles affecting Mono Lake in the Late Holocene. However, ancient shoreline records from ~12.0–4.0 kyr B.P. are poorly preserved or understudied, and therefore the history of environmental change at Mono Lake across the Pleistocene-Holocene transition is not well understood.

Compared to outcrop studies, examination of sediment cores retrieved from extant Mono Lake are less common. Most of the successful long coring that has taken place has been located in shallow water, where stratal completeness, sedimentation rates, and facies constrain the types of paleoenvironmental signals that can be extracted (Newton, 1994; Davis, 1999; Zimmerman et al., in press). In addition to the issue of erosion in shallow-water sites, the seismic reflection data of Colman et al. (2014) demonstrate that volcanic activity has disrupted many areas of the Mono Lake subsurface or deposited thick tephra layers, which makes the collection of intact strata from deeper water a challenge. However, those seismic data indicated sites in deepwater with minimally disturbed strata, which make attractive targets for coring due to their completeness, preservation state, and potential suite of paleoenvironmental proxies.

In this study, a new deepwater sediment core from Mono Lake's western embayment was used to assess late Quaternary paleolimnological changes. The coring location was guided by the seismic data of Colman et al. (2014); the result is the longest and most complete deepwater sediment core yet retrieved from the basin. We utilized the available paleoshoreline data to provide lake-level elevation context for interpreting changes in ancient limnological processes from the new core. Special emphasis is placed on elucidating the controls that shape deepwater stratigraphy and organic matter accumulation. Ecological studies conducted over the past several decades provide a framework for contextualizing organic carbon accumulation in Mono Lake sediments (Jellison and Melack, 1993a, 1993b; Jellison et al., 1993; Jellison et al., 1996). These studies inform the hypothesis that limnological changes control organic facies development over millennial timescales at Mono Lake. A multi-indicator approach was used to assess patterns of organic enrichment and infer the controls on productivity, preservation, and dilution dynamics in Mono Lake across the Pleistocene-Holocene transition and into the Early-Middle Holocene. The study adds key new paleolimnological data towards a more complete understanding of the late Quaternary history of the eastern Sierra Nevada region.

2. Setting

Mono Lake sits within the Mono Basin (~2070 km^2), a broad, shallow tectonic structure situated east of the Sierra Nevada in the Great Basin. The lake is located on the down-dropped block of the Lee Vining normal fault (Bailey, 2004). The high topography of the Sierra Nevada batholith forms the western flank of Mono Basin (Fig. 1). The mountains consist of Mesozoic granodiorites and include roof pendants of Paleozoic metasedimentary and metavolcanics rocks; these are the parent rocks for sediments entering Mono Lake via rivers from the west. To the east of the Sierras, Mono Basin is filled with Quaternary-aged lacustrine, alluvial, and glacial sediments, as well as Tertiary and Quaternary volcanic deposits (e.g., Reheis et al., 2002; John et al., 2012). The northern and southern margins of the Mono Basin consist of volcanic hills and the rim of the Long Valley Caldera (> Bailey et al., 1976; Hildreth, 2004). The Mono and Inyo Craters are prominent volcanic features adjacent to Mono Lake that consist of ~30 rhyolitic, dacitic, and rhyodacitic domes (Kelleher and Cameron, 1990; Marcaida et al., 2019). Tephras from Mono and Inyo eruptions have become

important for Quaternary geochronology and stratigraphic correlation in the Mono Basin (Lajoie, 1968; Stine, 1987; Benson et al., 1998; Zimmerman et al., 2006; Vazquez and Lidzbarski, 2012; Marcaida et al., 2019; Ali, 2018).

Precipitation in the Mono Basin is winter-dominant and varies with elevation. Mono Lake receives ~13 cm of precipitation annually, whereas snow and rainfall in the greater Sierras region can be as much as ~125 cm/yr. The annual temperature range is broad, with an average of ~−1 °C in January and ~21 °C in July. Mono Lake is fed by three streams with headwaters in the eastern Sierras: Rush Creek, Mill Creek, and Lee Vining Creek (Fig. 1). Under unaltered conditions, snowmelt from these streams contributes an estimated ~80% of the surface and groundwater inflow to the lake (Stine, 1990). However, the Los Angeles Aqueduct diverts much of the streamflow away from Mono Lake (e.g., Costa-Cabral et al., 2013). This water diversion program, which began in the 1940s, caused major changes in Mono Lake salinity, alkalinity, and ecology as water levels dropped > 14 m (Herbst, 1990; Stine, 1990; Stine, 1991; Jellison and Melack, 1993a).

Today, Mono Lake covers ~160 km^2, averages ~17 m deep, and has a shoreline elevation of ~1945 m a.s.l. (Jellison and Melack, 1993b). The lake is highly saline (87‰), alkaline (pH = 10.0), and its ion chemistry is dominated by Na^+, HCO_3^-, CO_3^{2-}, Cl^-, and SO_4^{2-} (Bischoff et al., 1991). Mono Lake is a warm monomictic lake that does not fully freeze over in the winter. Thermal stratification occurs in the spring and summer, whereas the lake mixes in the fall and winter, which drives nutrient cycling. Lake mixing can be affected by climate change, such as through unusual precipitation driven by the El Niño Southern Oscillation (ENSO). For example, heavy ENSO-related rainfall in 1982–83 increased the amount of freshwater delivered to Mono Lake, in part due to the forced release of water stored in Grant Lake reservoir, which led to chemocline formation and meromixis that lasted until 1988 (Jellison and Melack, 1993b; Jellison et al., 1993). Mono Lake's saline-alkaline chemistry controls its relatively simple food web. Algae in the lake include coccoid chlorophytes, coccoid cyanobacteria, and several bacillariophytes (Reed, 1977; Kociolek and Herbst, 1992; Wiens et al., 1993; Jellison et al., 1993; Newton, 1994; Herbst and Blinn, 1998; MacIntyre et al., 1999). The aquatic fauna are limited to nematodes, brine shrimp (*Artemia monica*), brine flies (*Ephydra hians*), which provide food for > 10^6 birds that use the lake for habitat during summer and early autumn (Wiens et al., 1993; Shih et al., 2019).

3. Methods

Sediment cores were collected from Mono Lake's western embayment in ~18-m-deep water at a position of latitude 37.99350°, longitude −119.12540° in October 2015. An UWITEC percussion piston corer was used to collect a sequential series of 2-m drives in the primary borehole (UWI-MONO15-1C). In order to cover gaps created by the piston within the core barrel, an adjacent borehole with staggered starting depths was also collected (UWI-MONO15-1D). Both boreholes were cored until refusal was met. Cores were transported to the National Lacustrine Core Facility at the University of Minnesota (LacCore) for physical properties scans, photography, initial description, and sub-sampling. High-resolution (0.5 cm) magnetic susceptibility (MS) readings were also collected on split cores using a Geotek MSCL-XYZ. The overlapping cores were correlated using distinct marker beds identified on high-resolution photos, as well as common patterns in MS data. The composite core (hereafter referred to as UWI-MONO15-1C/D), which is free of disturbances and gaps associated with the coring process, is ~10.81 m long. Core description and determination of lithostratigraphic units followed the techniques described in Schnurrenberger et al. (2003).

The chronology of UWI-MONO15-1C/D was determined using radiocarbon (^{14}C) and by correlation to tephras known from other studies (Table 1). ^{14}C dating was applied to plant macrofossils, charcoal, and pollen separates purified by flow cytometry, in order to avoid potentially spurious age dates that can be associated with bulk organic matter or lacustrine carbonates. Macrofossils and charcoal were sieved from the sediment during the initial core description. To build up the age-depth model, additional ^{14}C dates were obtained from pollen. Pollen was extracted from bulk sediments and sorted from refractory organic material via flow cytometer (Zimmerman et al., 2019, Tunno et al., in prep). Where sorted pollen concentrations exceeded 10,000 grains, the pollen were combusted into CO_2, graphitized and dated by accelerator mass spectrometry (AMS) at the Center for AMS at Lawrence Livermore National Laboratory. The base of the core contained considerable basaltic ash believed to be associated with the eruption of Black Point (Ash 2 of Lajoie, 1968), which sets the maximum age range at ~10.81 m to 17.2–19.1 kyr B.P. (Ali, 2018). A set of three Middle Holocene-aged tephras, uniquely correlative to those observed and dated via ^{14}C bracketing in the shallow water BINGO-MONO10-4A core, was also used in constructing the age model (Fig. 2) (Zimmerman et al., in press). The top of the core is interrupted by a thick sequence of coarse pumice and we do not attempt to extend our age model through this interval, given the likelihood of incomplete stratigraphy (Hodelka, 2018). Bacon, an R-based approach to age-depth modeling that applies Bayesian statistics to reconstruct sediment accumulation history, was used to produce the final age-depth model (Blaauw and Christen, 2011) (Fig. 3). Dates in Bacon were calibrated using the IntCal13 curve and the reported lithostratigraphic unit boundaries are weighted mean ages at the lower and upper contacts. Bacon was programmed to excise coarse-grained layers of tephra or sand ≥1 cm thick from the age-depth model ($n = 10$), as these deposits were most likely produced by abrupt, instantaneous events.

Discrete 1-cm thick sediment samples were collected every ~4 cm along the length of the core for total organic carbon (TOC), total nitrogen (TN), $\delta^{13}C_{ORG}$, $\delta^{15}N_{ORG}$, and biogenic silica (BiSi) analyses. These bulk geochemical data were used to determine accumulation patterns and environmental controls on organic matter through time (e.g., Meyers and Teranes, 2002). Sediment sub-samples ($n = 193$) were freeze dried and homogenized prior to analysis. To calculate carbonate-corrected TOC data, values of total carbon and total inorganic carbon (TIC) were measured at the University of Kentucky. Total carbon was determined using a Leco SC-144DR device, with a precision ± 1.0% based on replication of Leco standards 502–030 and 502–630. The TIC data were generated on a UIC CM5130 coulometer, which had a precision of ± 0.2% based on replicate analyses of pure $CaCO_3$. Values of TOC were calculated by subtracting TIC from total carbon. Stable-isotope measurements on bulk organic matter were made using an elemental analyzer coupled to a continuous-flow isotope-ratio mass spectrometer at the University of Utah. Precision for the $\delta^{13}C_{ORG}$ and $\delta^{15}N_{ORG}$ analyses was better than ± 0.2‰ based on an analysis of UU-CN-1, UU-CN-2, and Mt. Soil standards. Samples for the $\delta^{13}C_{ORG}$ analysis were digested overnight in ~30 mL of 1 N HCl to remove carbonate minerals; only the acid-insoluble fraction was used in $^{12}C/^{13}C$ measurements. The TN and $\delta^{15}N_{ORG}$ analyses were performed on untreated freeze-dried and homogenized sediment samples, due to the potential for fractionation or loss of nitrogen with acidification. Atomic C:N values were obtained through calculating the ratio of TOC values determined with the Leco and TN produced by the elemental analysis, multiplied by 1.167. $C{:}N_{ATM}$ data are widely applied in lake studies as an indicator of organic matter provenance (Meyers and Teranes, 2002). Insights on modern-sediment and -plant geochemistry were developed by measuring TOC, TN, $C{:}N_{ATM}$, $\delta^{13}C_{ORG}$, and $\delta^{15}N_{ORG}$ on three subaerial deltaic sediment samples from Rush Creek, and on 12 plant samples collected from the Rush Creek watershed. Core sediment samples from Mono Lake were also analyzed for BiSi (opal) at Northern Arizona University using molybdate-blue spectrophotometry (Mortlock and Froelich, 1989). The precision for this analysis was ± 1.0 wt%. Opal concentrations are routinely employed as a proxy for siliceous microfossil abundance and paleoproduction in lake core studies (Conley and Schelske, 2002). A table of all geochemical data generated in this

Table 1
Radiocarbon data and other age-control points used in the UWI-MONO15-1C/D age-depth model. Note that dates on tephras from BINGO-MONO10-4A core were acquired via ^{14}C and are discussed in Zimmerman et al., in press.

Lab #	Sample name	Depth (cm)	Material	Age (^{14}C yrs)	Error (±)	Age (cal yr BP)	2-σ range
177423	1C-2-1_54_55	205	Plant	3775	40	4150	3990–4290
N/A	Triplet 1*	224	Tephra	4365	85	4700	
N/A	Triplet 2*	228	Tephra	4700	450	5100	
N/A	Triplet 3*	234	Tephra	5065	610	5400	
176259	1C-2-2_45.7	296.3	Plant	5740	30	6540	6450–6630
173692	1D-2-1_67	307.4	Plant	6300	70	7225	7020–7420
173693	1D-2-2_3.5	314	Plant	6350	45	7285	7170–7420
173695	1D-2-2DUP_3.5	314	Plant	6150	40	7060	6940–7160
177425	1D-2-2_5.4_6.4	316.4	Plant	6620	110	7510	7430–7680
176260	1D-2-2_26_27	337	Charcoal	8850	100	9930	9610–10,200
173694	1D-2-2_33.5	344	Plant	7070	70	7890	7740–8010
178075	1D-2-2_42.4	353	Pollen	8220	240	9150	8520–9680
118472	1D-2-2_43	354	Pollen	8140	240	9060	8460–9540
176261	1D-2-2_57.3	367.7	Plant	8610	180	9660	9160–10,190
177392	1C-3-2_26.6	421.5	Plant	10,070	570	11,640	10,190–13,060
177393	1C-3-2_27.3	422.2	Plant	9910	410	11,460	10,300–12,600
177394	1C-3-2_29.4	424.3	Plant	10,010	570	11,570	9960–13,030
177395	1C-3-2_64.9	459.8	Plant	9400	70	10,630	10,410–11,070
177396	1C-3-2_102.4	497.3	Plant	11,110	600	12,940	11,220–14,520
178076	1D-3-2_31	503	Pollen	10,090	130	11,670	11,240–12,120
178074	1C-4-2_39.5	653	Pollen	12,650	390	14,920	13,760–16,080
179010	1D-5-2_93.5_94.5	952	Pollen	12,740	220	15,110	14,210–15,800
N/A	Black point	1082	Tephra	na	na	17,200	15,300–19,100

study appears in the online supplemental materials (Supplemental Materials Table 1).

4. Results

4.1. Chronology and lithostratigraphy

The Bacon-derived age model for UWI-MONO15-1C/D consists of 19 horizons dated using ^{14}C (inclusive of three horizons with replicates) and four tephra correlations (Fig. 3) (Table 1). Correlation to a package of three thin tephras in the BINGO-MONO10-4A core (Zimmerman et al., in press) provide additional age control from ~5.4–4.7 kyr B.P. (Fig. 2). Three dates that were out of stratigraphic order were excluded by the Bacon modeling algorithm. The age of the base of the core is constrained by the presence of what is interpreted to be Black Point basaltic tephra, which has a characteristic brown color (Munsell 10YR 4/3) and velveteen texture (Fig. 4). Though Black Point is known to have erupted several times, Bailey (2004) notes that the initial eruption was subaqueous and produced brown palagonitized tephra, whereas the younger eruption was subaerial and produced glassy black ejecta. With these assumptions in mind, the age model defines two long term sedimentation rates: ~0.11 cm/yr for the late Pleistocene, and ~0.05 cm/yr for the Holocene. Our geochemical sampling therefore typically resolves changes averaged over several decades to centuries.

The stratigraphy of UWI-MONO15-1C/D is shown in Fig. 4. The core can be divided into seven lithostratigraphic units from oldest (I) to youngest (VII). This study focuses on units I to V, which represent the Pleistocene-Holocene transition. Units I and II capture sedimentation in the late Pleistocene, while Units III-V were deposited during the Early and Middle Holocene. Units I through V consist of well-preserved lacustrine muds and tephras of varying grain size, with occasional layers of siliciclastic sand (Fig. 4). Units I and II contain most of the coarse detrital layers in the core, which generate high MS readings due to an association with ferromagnetic grains (Fig. 5). Typically, coarse detritus is organized as beds, laminations, or lenses of sand-sized siliciclastic detritus or tephra (Figs. 4, 6). Discrete pebbles that disrupt bedding were encountered in Units I and II (Fig. 6). The background MS is higher in Units I and II in comparison to the overlying strata (Fig. 5), which is best explained by elevated silt content observed on smear slides. Occasional MS spikes occur in Units IV and V, which correlate with discrete thin beds or laminations comprised of fine sand or coarse silt.

Sediment color and laminae character are very different in the late Pleistocene versus Holocene muds of the UWI-MONO15-1C/D core (Figs. 6, 7). Units I and II consist of brown-grey (10YR 6/2), dark blue-grey (5PB 3/1) and black (N 2.5/1) lacustrine sediments, whereas coarse detritus is black or grey-white (Fig. 6). Lacustrine muds in Unit I are typically structureless, whereas in Unit II, muds are organized into occasional lamination sets, thin beds (1–3 cm thick), or more massive beds. Where laminations are present, they are planar and vary from continuous to discontinuous (Fig. 6). Unit III shows a marked change in color, transitioning from black and grey laminated muds to dark red-brown (2.5YR 4/1), olive (5Y 5/2) and grey laminated muds beginning ~12.2 cal kyr BP (Fig. 6). Laminations and thin beds in Unit III are planar and continuous. Units IV and V consist chiefly of olive (5Y 5/4), olive-brown (2.5Y 4/3), and blue-grey (5PB 4/1) laminations and thin beds (Fig. 7). Unit IV laminations are highly diverse. Many laminae in Unit IV are remarkably thin (sub-mm), planar, and continuous, whereas others contain mm-scale tan-yellow calcareous blebs along bedding planes. Unit Va laminations are typically thicker (up to 2 mm) with diffuse contacts (Fig. 7). Some laminae in Unit Va consist of coarse ungraded sediment (Fig. 7). Smear slides and thin sections reveal that these coarse laminae consist of tufa rubble, ostracodes, and siliciclastic detritus. Unit Vb laminations are dark yellow-brown muds with variably diffuse or sharp contacts.

4.2. Geochemistry

4.2.1. Modern sediments and plant material

Modern sediments from the Rush Creek delta have low TOC concentrations (0.11–0.63 wt%) and average $\delta^{13}C_{ORG}$ and $\delta^{15}N_{ORG}$ values of −26.3‰ and 3.9‰, respectively (Table 2). The $\delta^{13}C_{ORG}$ data exhibit < 2.0‰ variability, whereas $\delta^{15}N_{ORG}$ ranges from ~2.9–5.7‰. The isotope data for plant samples in the Rush Creek drainage vary widely, from −31.7‰ to −15.5‰ ($\delta^{13}C_{ORG}$) and −5.7‰ to 4.6‰ ($\delta^{15}N_{ORG}$). The highest $\delta^{13}C_{ORG}$ value for modern plants was from *Poaceae* spp. (C_4), whereas C_3 trees generally had lower values. The $C:N_{ATM}$ range for the modern plants was 11–64.

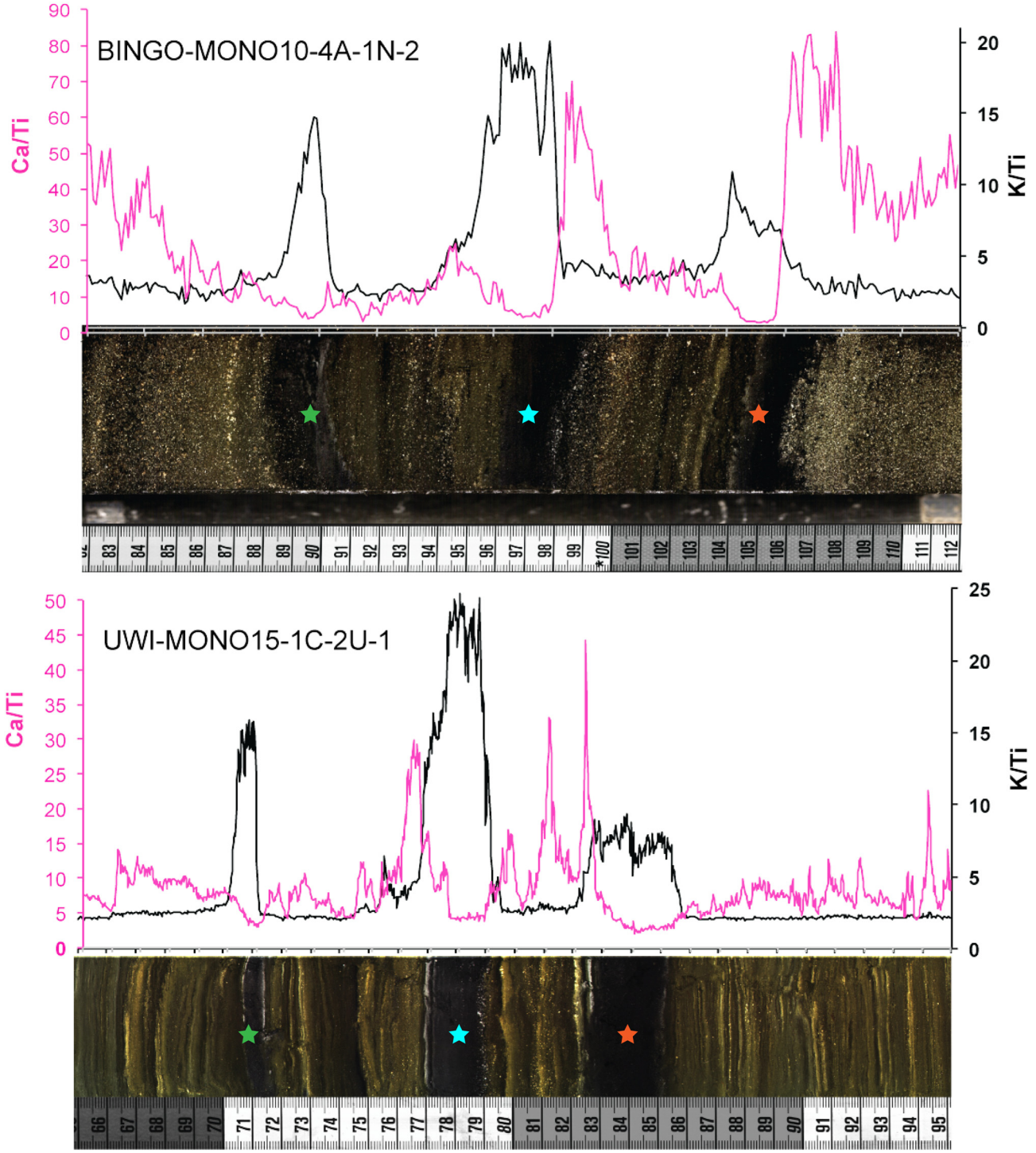

Fig. 2. Three thin tephra layers used for age control in the UWI-MONO15-1C/D age-depth model. Upper panel shows the tephra layers in the BINGO-MONO10-4A-1N-2 core section. The tephras exhibit characteristic peaks in K/Ti, and are separated stratigraphically by relatively high Ca/Ti muds. Age estimates for these tephra layers based on surrounding ^{14}C are 5065 ± 610, 4700 ± 450, and 4365 ± 85 kyr B.P. (Zimmerman et al., in press). The lower panel shows what we interpret as equivalent tephras, with similar geochemical patterns, in the UWI-MONO15-1C-2U-1 core section.

4.2.2. Late Pleistocene-Holocene sediments

Unit I (~16.6–15.9 cal kyr B.P.) has uniformly low TOC (0.09–0.14 wt%) and some of the highest BiSi concentrations (17.0–23.0 wt%) in the record (Fig. 5). Unit I $\delta^{13}C_{ORG}$ values range from −26.8‰ to −23.9‰ and increase towards the top of the unit. Values of TN were very low in Unit I (< 0.1 wt%) and only three $C:N_{ATM}$ data points (9–13) could be determined (Fig. 5). The $\delta^{15}N_{ORG}$ values range from −3.0 to 7.0‰, increasing towards the top of the unit.

Unit II consists of two sub-units. Unit IIa (~15.9–13.9 cal kyr B.P.) exhibits low to moderate TOC and low to moderate BiSi concentrations that vary around means of ~0.9 wt% and ~7.5 wt%, respectively (Fig. 5). $\delta^{13}C_{ORG}$ values vary by ~8.0‰ in Unit IIa, and values approach ~−30.0‰ near the upper contact (Fig. 5). $\delta^{15}N_{ORG}$ values are generally high, with a decreasing trend moving up section, with values ranging from 2.0–10.0‰. The $C:N_{ATM}$ values in Unit IIa vary from 8 to

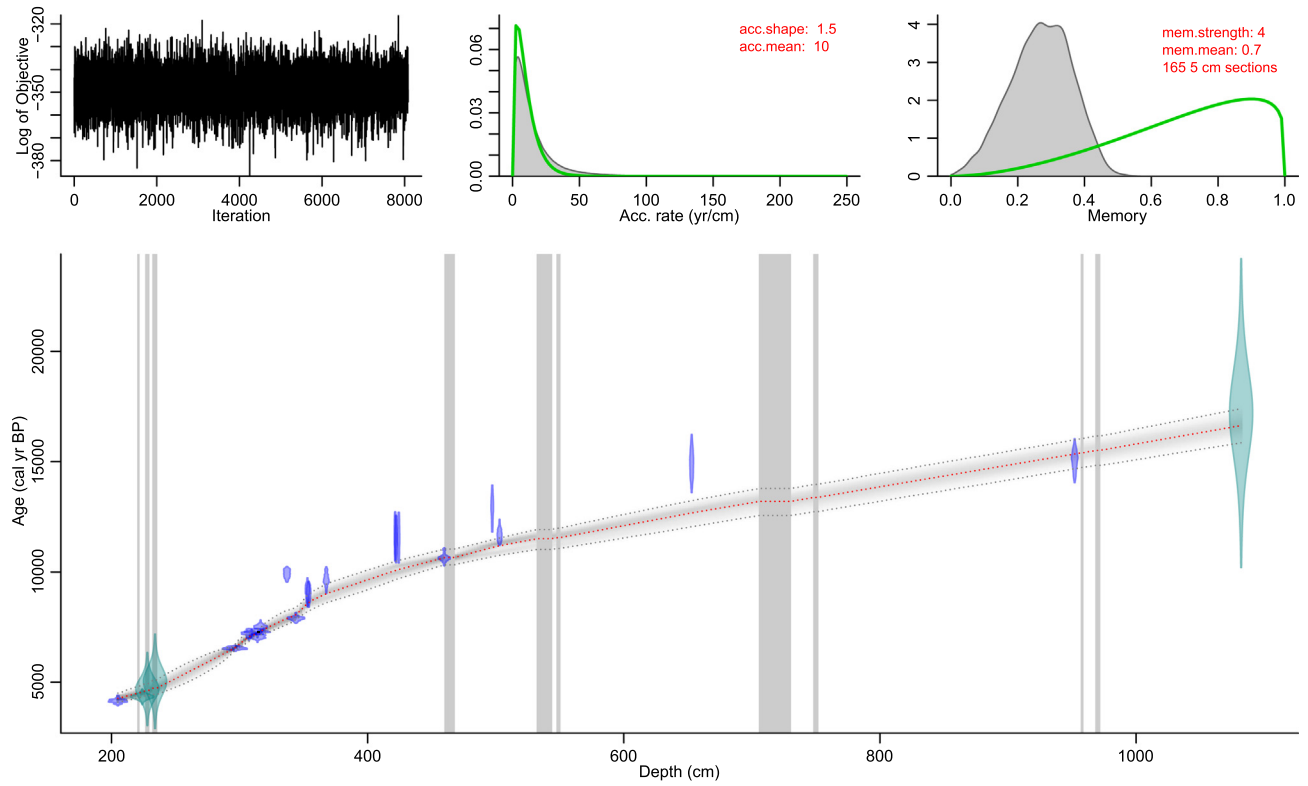

Fig 3. Bacon-derived age-depth model for the UWI-MONO15-1C/D core. The vertical grey bars ($n = 10$) mark the position of sand and tephra layers ≥ 1 cm thick that have been modeled as events of instantaneous deposition. These beds occur at 971.5–968.7 cm, 958.3–957.3 cm, 751.4–748.5 cm, 730–706 cm, 550–548 cm, 543.5–532.5 cm, 467.5–460.5 cm, 235.2–232.5 cm, 229–226.9 cm, and 221.4–220.7 cm. See text for details.

30, with an average value of ~13.

TOC values in Unit IIb (~13.9–12.8 cal kyr B.P.) are only slightly elevated in comparison to underlying sediments and have a mean of 1.0 wt%, whereas the mean BiSi concentration (~10.0 wt%) increases by ~2.0 wt%. $C:N_{ATM}$ values vary from 6 to 15, with an average value of ~12 (Figs. 5, 8). The $\delta^{13}C_{ORG}$ and $\delta^{15}N_{ORG}$ curves exhibit sawtooth patterns with minor variability in Unit IIb, with values that average ~ −28.0‰ and 5.0‰, respectively (Fig. 5).

Unit III (~12.8–10.9 cal kyr B.P.) sediments exhibit variable TOC concentrations (0.5–9.0 wt%) that generally increase upward, with several prominent peaks near the upper contact (Fig. 5). These peaks are the highest in the UWI-Mono15-1C/D core. The BiSi are likewise highly variable (3.0–19.0 wt%), showing a sawtooth pattern (Fig. 5). The vertical pattern in $C:N_{ATM}$ displays a clear increase towards the upper contact in Unit III, with values ranging from 12 to 22. The $\delta^{13}C_{ORG}$ values range between −28.0 to −23.0‰ and gradually become more positive up section. Similarly, $\delta^{15}N_{ORG}$ also increases towards the upper contact, with values between 4.0 and 15.0‰; prominent peaks occur after ~11.8 kyr B.P. (Fig. 5).

Unit IV (~10.9–8.6 cal kyr B.P.) has relatively low TOC concentrations (mean = ~2.0 wt%) that increase slightly upward. BiSi values in Unit IV vary (~5.0–15.0 wt%) but generally decline towards the upper contact (Fig. 5). Similarly, $C:N_{ATM}$ values decline upward, varying between 12 and 17. The $\delta^{13}C_{ORG}$ values range from −25.0 to −23.0‰ and become more positive up section. The $\delta^{15}N_{ORG}$ values range from 3.0 to 6.0‰ and likewise increase up section (Fig. 5).

Unit V consists of two sub-units. The TOC concentrations (mean = 2.0 wt%) display a slight increase towards the top of Unit Va (~8.6–6.3 cal kyr B.P.), whereas the BiSi values range from 3.0–11.0 wt % and show a slight decrease upward (Fig. 5). $C:N_{ATM}$ values are slightly higher than those of the underlying unit (Fig. 8). Excluding a single outlier, the $C:N_{ATM}$ values show minor variability with a slight decrease upward. Muds from Unit Va exhibit minor variability in $\delta^{13}C_{ORG}$ (−24.0 to −20.0‰) and $\delta^{15}N_{ORG}$ (4.0–8.0‰), with both isotopes becoming enriched towards the upper contact (Fig. 5).

Unit Vb (~6.3–4.3 cal kyr B.P.) exhibits TOC concentrations (mean = 3.0 wt%) that are higher than Unit Va; values increase and become highly variable towards the upper contact. The BiSi concentrations in Unit Vb decrease towards the upper contact, with values ranging from 4.0–13.0 wt%. $C:N_{ATM}$ values are relatively invariant and range from 13 to 6. The muds from Unit Vb exhibit slightly less variability in $\delta^{13}C_{ORG}$ (−24.0 to −21.0‰) relative to Unit Va, whereas $\delta^{15}N_{ORG}$ variability is similar to Unit Va (Fig. 5).

5. Discussion

5.1. Overview

We adopted the late Pleistocene paleo-shoreline chronology of Ali (2018) and core-based insights on Holocene hydroclimate from the eastern Sierra Nevada (including shallow water sediments in Mono Lake; Davis, 1999; Zimmerman et al., in press) as context for interpreting how the principle controls on organic facies, namely primary production, preservation dynamics, and dilution (Bohacs et al., 2000), varied in Mono Lake ~16.6–4.3 cal kyr B.P.. A conceptual model for the lake's paleogeographic configurations during this period appears in Fig. 9, which was informed by prior publications on the extent of glaciers in the eastern Sierras during the late Pleistocene (Rood et al., 2011).

The strong positive correlation between carbon and nitrogen for all units in the core demonstrates that the geochemical data reflect changes in organic, rather than inorganic, sources (Fig. 8) (Talbot, 2002). We track changes in organic matter burial via the TOC chemostratigraphy, and relative diatom production through the BiSi. Post-depositional oxidation of organic matter can influence the fidelity of limnological reconstructions using TOC alone, and therefore we relied on multiple

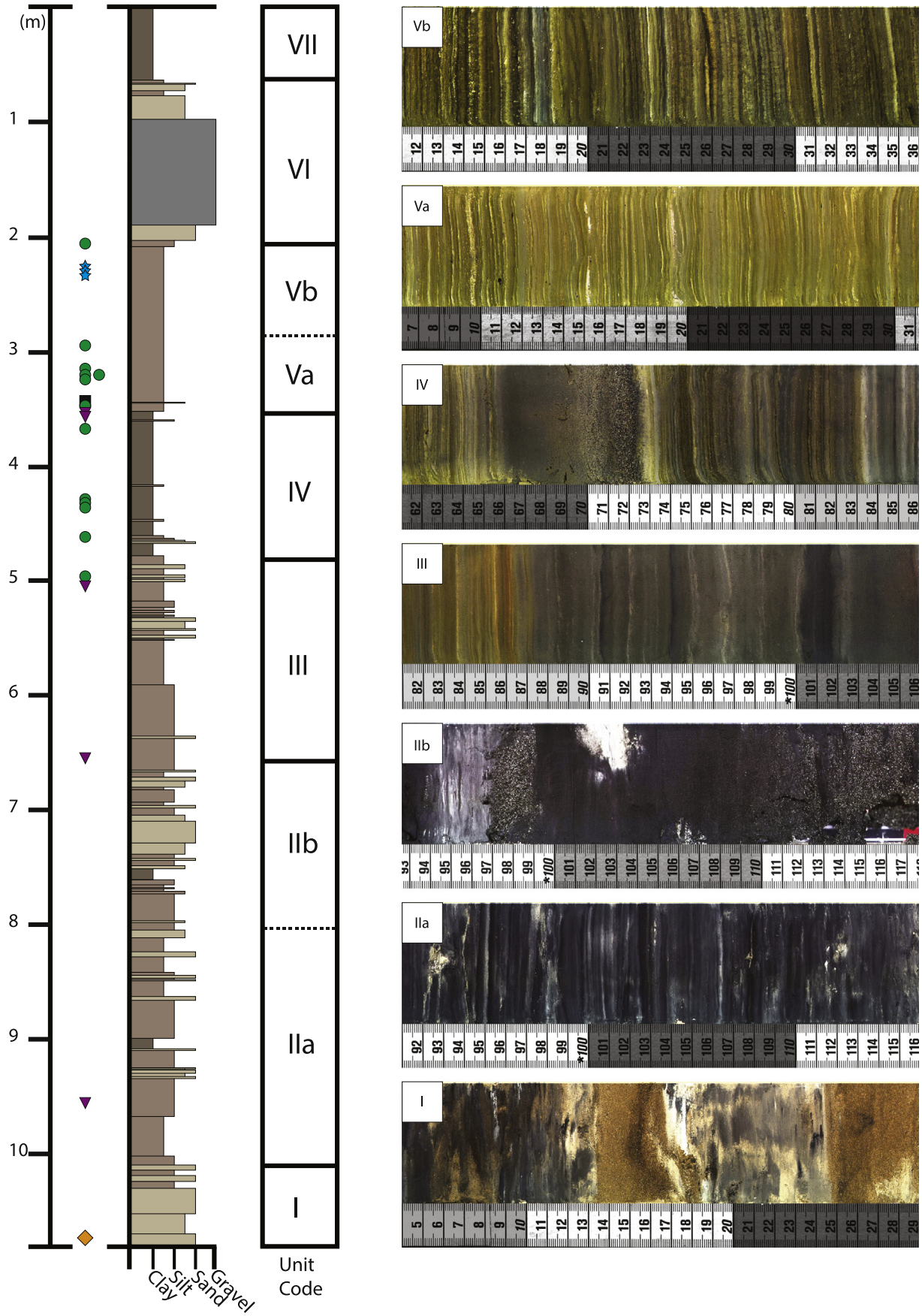

(caption on next page)

Fig. 4. (Left) Stratigraphic log of the 10.81 m composite UWI-Mono15-1C/D core with the location of ^{14}C-dated horizons. Green circles, plant macrophytes; blue stars, correlated dates from tephras known from other studies in the Mono Basin; black square, charcoal fragments; purple triangles, pollen concentrate; orange diamond, Black Point tephra. (Right) Interpreted lithostratigraphic units and representative core photos. In all photos, the top of the core is to the left and the scale is in centimeters. (For interpretation of the references to color in this figure legend, the reader is referred to the web version of this article.)

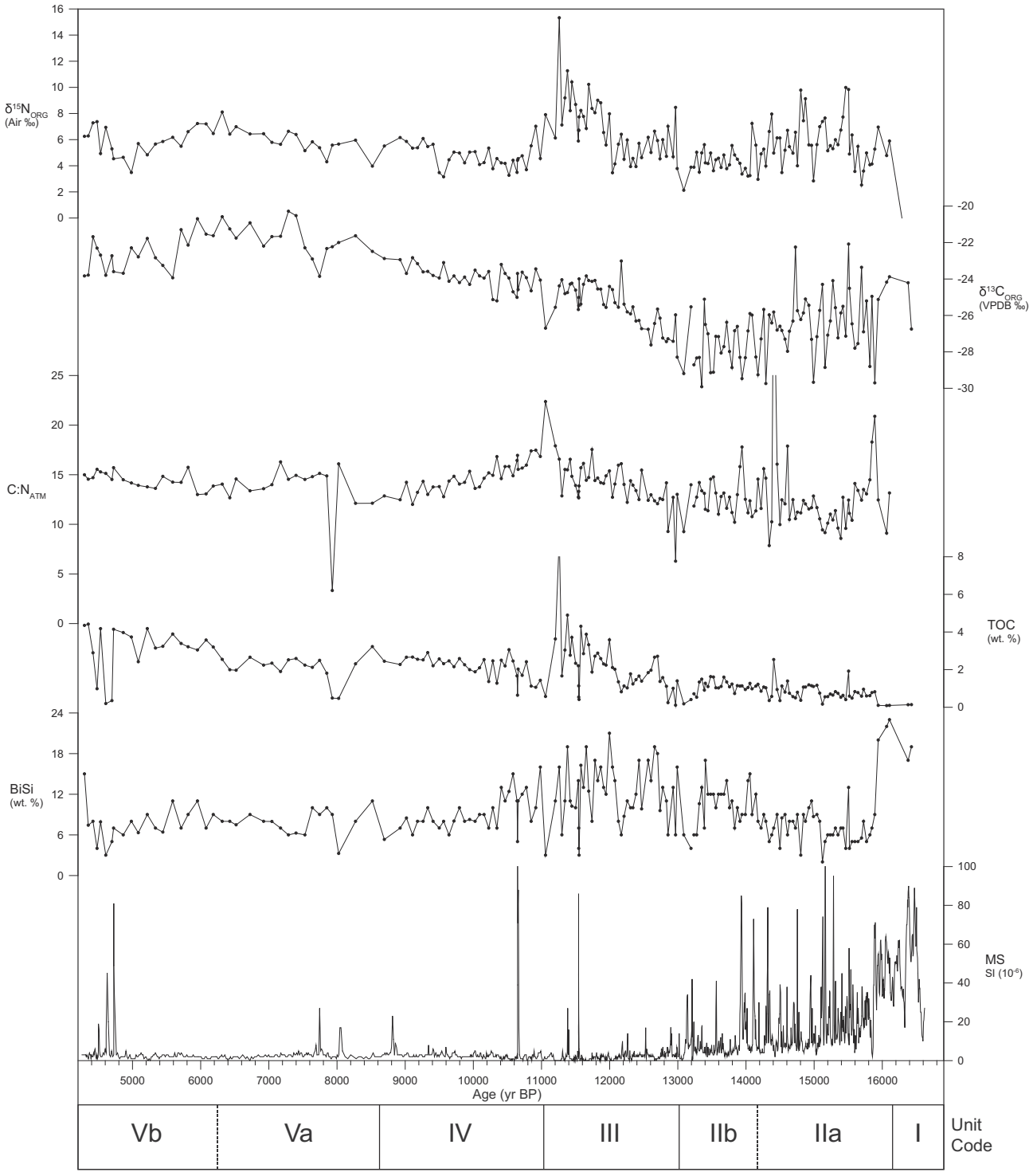

Fig. 5. Multi-indicator chemostratigraphy for the UWI-MONO15-1C/D core. Lithostratigraphic unit boundaries are shown on the horizontal axis below age/depth information. See text for details.

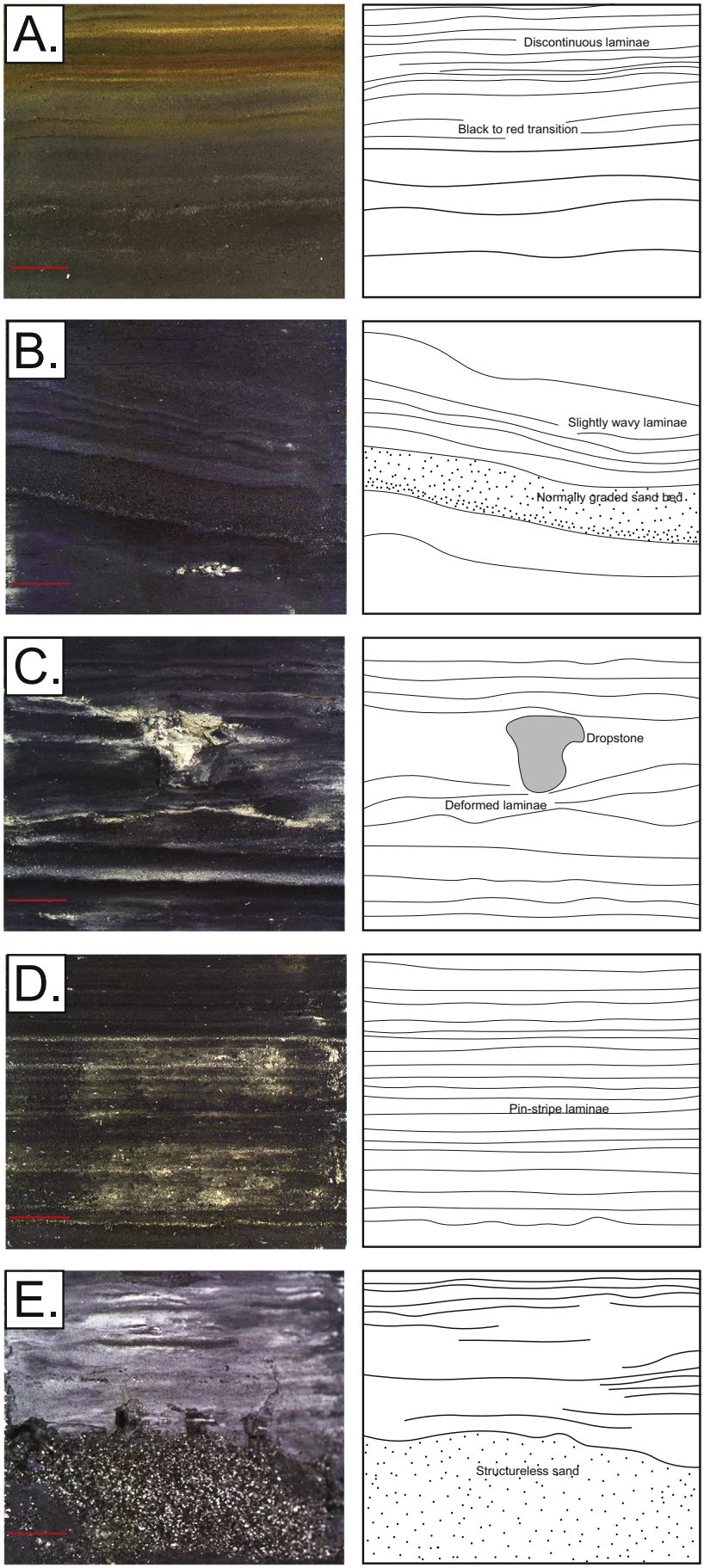

Fig. 6. Sedimentological features of late Pleistocene strata from deepwater Mono Lake. Scale bar is 1 cm. (A) Pleistocene-Holocene transition with mud color change from black to red. Note the presence of discontinuous laminations in this section, possibly related to lake floor reworking. (B) Normally graded sand bed overlain by tilted, slightly wavy laminae interpreted as a turbidite. (C) Bedding-deforming pebble dropstone provides evidence of detritus-containing lake ice. (D) Very fine pin-stripe laminations characteristic of highstand deposits, here from the Younger-Dryas. (E) Ungraded structureless sand bed potentially related to slumping or volcanic eruption. (For interpretation of the references to color in this figure legend, the reader is referred to the web version of this article.)

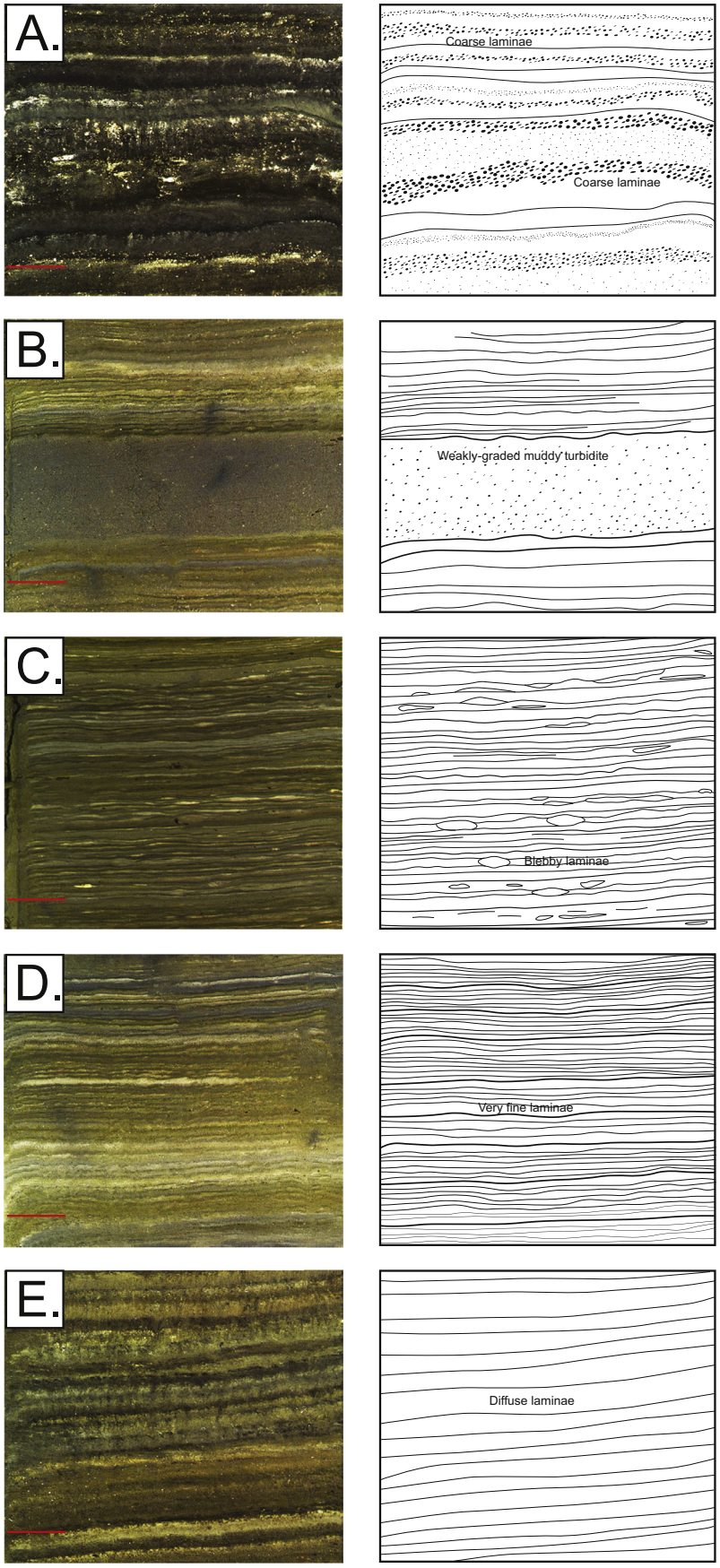

Fig. 7. Sedimentological features of Early and Middle Holocene strata from deepwater Mono Lake. Scale bar is 1 cm. (A) Coarse lamination comprised of ostracods, tufa, and terrigenous detritus interpreted as wave reworked nearshore material deposited offshore. (B) Weakly graded, low to moderate MS, muddy turbidite. These features may have resulted from sub-lacustrine slope failures, or due to floods that carried Wilson Creek Formation muds to the lake. (C) Blebby laminae. Smear slides show that blebs consist of fine-grained carbonate. (D) Very fine lamination of Unit IV, likely indicating lake floor anoxia. (E) Diffuse laminae likely created via periodic ventilation or bioturbation of the lake floor.

Table 2
Geochemical data for modern sediments and plants collected from the Rush Creek delta region.

Sample	δ^{13}CORG (‰ VPDB)	δ^{15}NORG (‰ Air)	C:N (ATM)	TOC (wt%)	TN (wt%)
T9-1-1B (sediment)	−26.85	2.85	18	0.63	0.04
T9-7-3B (sediment)	−26.81	3.17	15	0.38	0.03
T9-8-1B (sediment)	−25.26	5.68	12	0.11	0.01
Artemisia arbuscula	−26.81	3.00	38	45.5	1.38
Chrysothamnus spp.	−26.70	−1.07	43	47.6	1.29
Eriogonum umbellatum	−26.41	1.18	31	42.6	1.61
Lupinus spp.	−28.81	2.41	11	41.8	4.27
Pinus jeffreyi	−24.26	0.98	64	47.2	0.86
Populus spp.	−27.52	−2.51	26	43.8	1.95
Purshia tridentata	−26.03	−2.29	35	47.3	1.58
Rosa spp.	−28.62	−1.83	30	42.3	1.64
Salix spp. "*dark salix*"	−28.51	−5.74	38	45.2	1.40
Salix spp.	−31.73	4.65	45	43.8	1.14
Typha spp.	−27.29	2.73	38	40.2	1.24
Poaceae spp.	−15.47	1.38	30	40.9	1.60

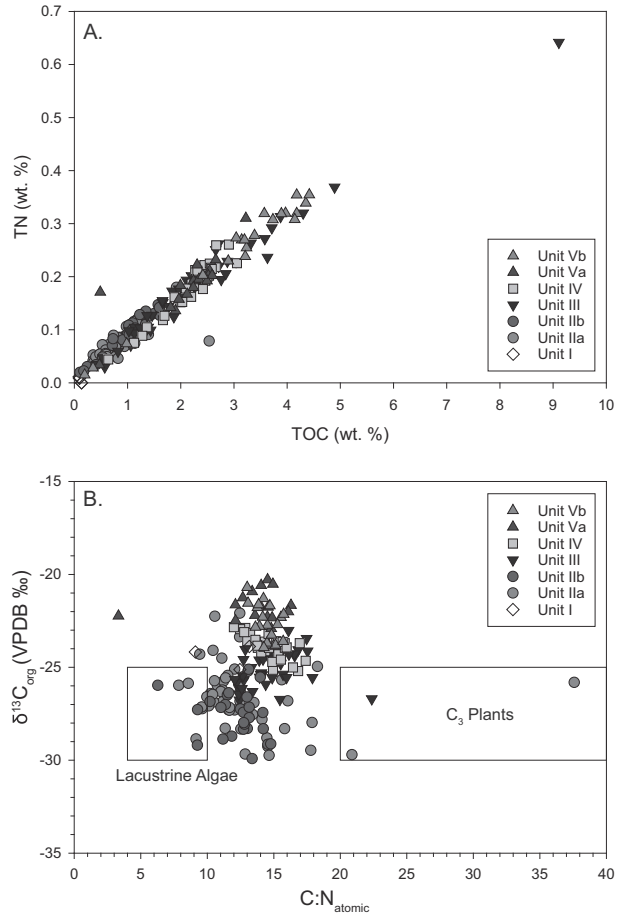

Fig. 8. (A) Total organic carbon (TOC) versus Total Nitrogen (TN). The strong positive correlation between TOC and TN, coupled with an intercept at unity indicates that only organic sources contribute to these values (Talbot, 2002). (B) $C:N_{ATM}$ versus $\delta^{13}C_{ORG}$ cross plot illustrates the source of organic matter for each lithostratigraphic unit. Fields for C_3 plants and lacustrine algae adapted from Meyers and Teranes (2002).

geochemical indicators to infer periods of elevated algal productivity (Meyers and Lallier-Verges, 1999). Low $C:N_{ATM}$ suggests the dominance of algal organic provenance. In contrast, time intervals influenced by transport of terrestrial or nearshore macrophyte organic material to the core site were identified with high relative $C:N_{ATM}$ (Fig. 8), and via comparisons to modern plant $\delta^{13}C_{ORG}$ and $\delta^{15}N_{ORG}$ data from the Rush Creek watershed (Table 2). In large lakes, changes in the rate of primary production have been interpreted using $\delta^{13}C_{ORG}$, which increases through preferential uptake of ^{12}C by algae during photosynthesis (e.g., Hodell and Schelske, 1998). McFadden et al. (2004) noted that $\delta^{15}N_{ORG}$ may increase with higher rates of primary production, due to preferential uptake of ^{14}N by algae, though changes in the dissolved inorganic nitrogen (DIN) pool or diagenesis can also influence the isotope value of aquatic source material (Talbot and Johannessen, 1992).

5.2. Late Pleistocene (Units I and II, ~16.6–15.9 cal kyr B.P. and ~15.9–13.9 cal kyr B.P)

Late Pleistocene lake sediments in the UWI-MONO15-1C/D are dark colored, intermittently laminated, and contain relatively abundant silt and sand (Fig. 4); these are best represented in Units IIa and IIb, because Unit I is mostly Black Point ash (Bailey, 2004). The other prominent late Pleistocene-aged ash from the Mono Basin, the rhyolitic Ash 1 of Lajoie (1968), has proven more challenging to unequivocally identify in UWI-MONO15-1C/D. Several candidates exist, but chemical fingerprinting of titanomagnetites (Marcaida et al., 2019) is needed before this layer can be incorporated in the age-depth model.

Unit I lacustrine sediments were most likely deposited during the deglacial highstand that occurred in Mono Lake ~18.5–16 kyr B.P. (Ali, 2018). A paleoecological analysis completed by Forester (1987) showed that lake sediments encasing the Black Point ash in the WCF contained ostracods that thrive in dilute lake water, which supports the interpretation of high water levels at Mono Lake during this time (Ali, 2018). Relatively low $C:N_{ATM}$ and $\delta^{13}C_{ORG}$ values signal that algae (C_3) were likely the primary source of organic matter to Unit I sediments (Fig. 8). Smear slides indicate the presence of diatoms, and together with elevated BiSi concentrations, the data suggest a relatively productive Mono Lake during the highstand. Dark mud colors and the intermittent laminations suggest the potential for reducing conditions at the sediment-water interface, which typically favor the preservation of organic matter by limiting bioturbation and re-mineralization via oxidation. However, the lack of pervasive fine laminations suggest that bottom waters were most likely neither persistently anoxic, nor strongly influenced by seasonal or annual cycles of sedimentation. Yet the very low TOC concentrations, high MS, and high Pleistocene sedimentation rates point towards dilution as the primary control on organic facies development in Unit I. In this interval, the most important dilutant was altered tephra from the initial Black Point eruption.

A regression that lowered the water level elevation at Mono Lake by ~140 m began ~16.0 kyr B.P. and ended ~14.0 kyr B.P. (Ali, 2018). Thus, Unit IIa was deposited chiefly during a falling stage of lake level. Unit IIa stands out for its relatively high and variable MS, $C:N_{ATM}$, $\delta^{15}N_{ORG}$ (Fig. 5). Laminae-deforming pebbles were encountered in Unit IIa, but the high average MS values are attributed to silt content within

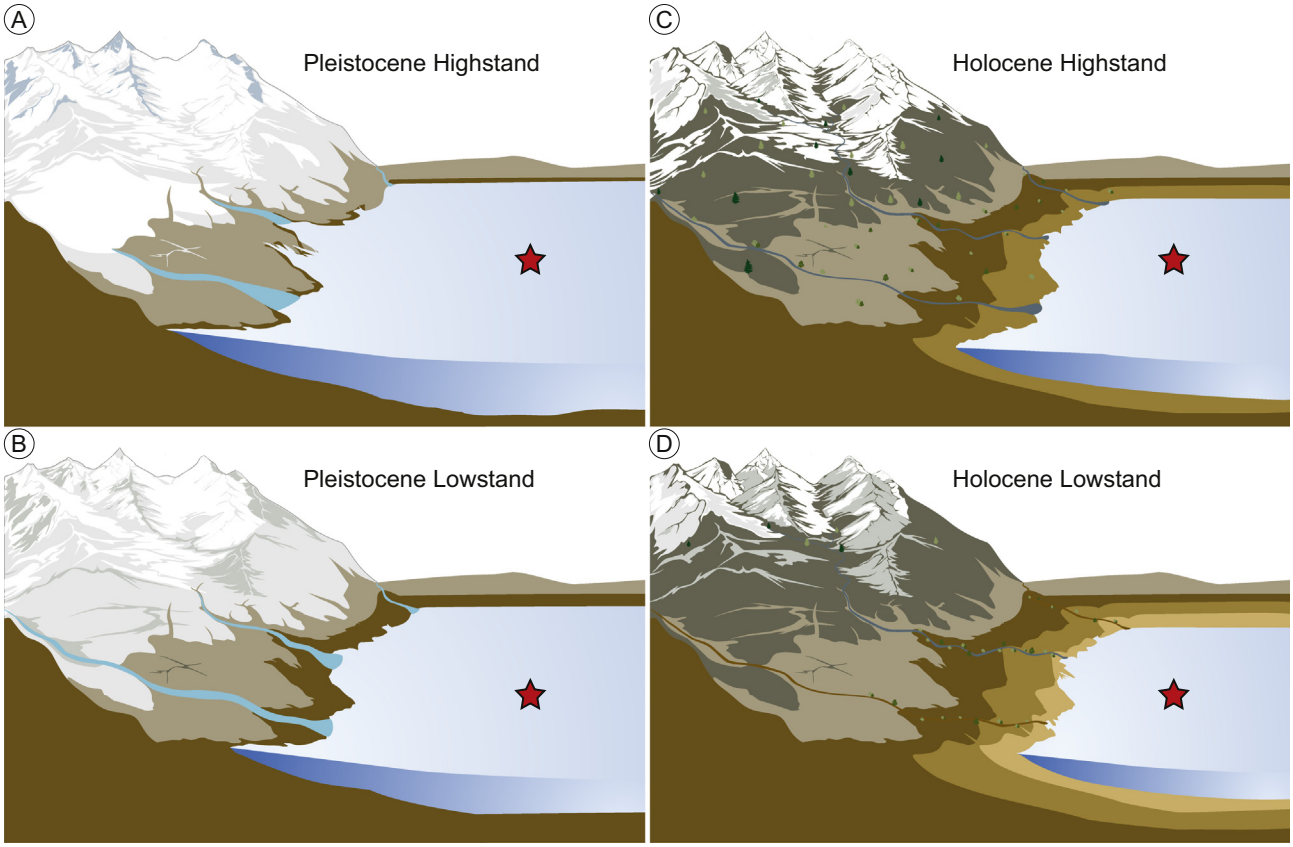

Fig. 9. Paleogeographic sketch maps for the Pleistocene-Holocene transition at Mono Lake. Expansive glaciers present in the Pleistocene influenced organic facies through the delivery of silt to the lake via east-flowing rivers, and lake level was much higher prior to Holocene. The proximity of the core site (stars mark the approximate location) to the shoreline and wave reworking processes were important to organic facies development during Holocene lowstands. By contrast, water column stratification and low lake floor oxygen were important influences during highstands. (A) Mono Lake at highstand during the Pleistocene. (B) Mono Lake at lowstand during the Pleistocene. (C) Mono Lake at highstand during the Holocene. (D) Mono Lake at lowstand during the Holocene.

laminated to thinly bedded black and dark grey muds; this silt was most likely from newly exposed WCF deposits, generated by glacial erosion of Sierran bedrock. Large MS peaks most commonly occur due to the presence of thin beds of coarse silt, sand, and volcanic glass, which exhibit normal grading (Fig. 5). We interpret these beds as turbidites, most likely associated with the development of hyperpycnal flows from river plumes. $C{:}N_{ATM}$ is > 20 at several horizons in Unit IIa, and we interpret these values to reflect elevated contributions of terrestrial organic matter to offshore depositional environments (Meyers and Lallier-Verges, 1999) (Fig. 8). It is plausible that allochthonous organic matter was transported to the core site by hyperpycnal flows; similar processes have been interpreted for other lakes (e.g., Sturm and Matter, 1978; Osleger et al., 2009; Howarth et al., 2012). This process may also affect bulk $\delta^{13}C_{ORG}$, which is highly variable in Unit IIa, if a mix of C_3 and C_4 plants were present in the watershed. Based on the low to moderate TOC and BiSi concentrations (Fig. 5), we interpret that primary productivity was relatively low and the effects of dilution were important to organic facies development in Mono Lake ~15.9–13.9 cal kyr B.P. We note that the study of Jellison et al. (1996) indicated that over the last ~170 yrs, sedimentary TOC at Mono Lake increased when lake levels declined, potentially due to higher lake water salinity that inhibited the microbial remineralization of organic matter. We do not find evidence of a similar relationship during Unit IIa time, though high $\delta^{15}N_{ORG}$ suggest the possibility of ammonia volatilization at relatively high pH, a mechanism used to explain lake water ^{15}N enrichment during lowstands in other lakes (Talbot and Johannessen, 1992). Our analysis of smear slides, however, suggests that evaporite minerals were not abundant in this interval, and therefore a highly concentrated brine is less likely. A likewise plausible explanation for the high $\delta^{15}N_{ORG}$ is a shift in phytoplankton assemblage and subsequent drawdown of a limited DIN pool (Talbot, 2002).

The presence of turbidites in Unit IIa is consistent with the low water level elevation of Mono Lake ~16.0–14.0 cal kyr B.P. reported by Ali (2018). The work of Stine (1990) showed that regressions in Mono Lake triggered down-cutting of east-flowing Sierran streams, and following this analog, we infer that incision and basinward progradation of deltas occurred in Unit II time. The mean $\delta^{13}C_{ORG}$ values for modern sediments and plants from Rush Creek delta and Unit IIa deposits are similar (−26.4‰ versus −26.9‰), which is consistent with our interpretation. Organic richness in lake deposits often declines in depositional environments proximal to debouching deltas due to dilution and water column turbidity that limits photosynthesis (Ellis et al., 2015; McGlue et al., 2015). Given the geochemistry of Unit IIa, it is possible that algal productivity was limited by reduced light penetration. By analogy, Benson et al. (2003b) indicated that high turbidity may have limited productivity in nearby Owens Lake during the late Pleistocene. In Unit IIa, we interpret laminae-deforming pebbles as dropstones (e.g., Bennett et al., 1996), which indicate that lake ice transported coarse nearshore detritus to offshore depositional environments (Zimmerman et al., 2011b). This process, along with glacial flour transported by incising streams, likely helped to limit organic richness in Unit IIa.

TOC, $\delta^{13}C_{ORG}$, and MS data for Unit IIb (~13.9–12.9 cal kyr B.P.) indicates that paleo-production was relatively low, and that dilution influenced organic richness. In addition to pebble dropstones, Unit IIb contains a unique package of black, thick-bedded, upward-fining sand with intercalated mud lenses (Fig. 4). Smear slides indicate the sand consists of quartz and volcanic glass, with minor whole and fragmented ostracodes; muddy sands at the top of the package are calcareous. We

interpret this deposit as a slump that formed by the collapse of a low-stand delta front, and this feature was accounted for in the age-depth model (Fig. 3). Numerous geological processes can lead to delta collapse and sub-lacustrine mass wasting (e.g., Girardclos et al., 2007). The paleoshoreline chronology of Ali (2018) indicates that Mono Lake was at mostly at lowstand during the deposition of Unit IIb, and we favor falling lake level and associated pore pressure instabilities as the best explanation for the existence of this deposit. However, we cannot rule out that a volcanic eruption with associated seismicity was responsible for deltaic collapse, given the relative abundance of volcanic glass within the sand. A less likely alternative interpretation is that of a littoral zone deposit, but the presence of intercalated muddy lenses argue against deposition in very shallow water influenced by wave agitation, which entrain and carry fine-grained sediments offshore (Håkanson, 1982). Moreover, a water level elevation of ~2015 m asl is suggested by the mapping of Ali (2018), which places the core site in the western embayment in deepwater at this time.

The timing of Unit IIb overlaps with the Bølling-Allerød (B-A), which generally marks the end of the last glacial period (Weaver et al., 2003). Evidence for environmental change around the B-A has been reported previously for the eastern Sierra Nevada. For example, sediment and paleo-vegetation datasets support the interpretation that low lake levels and drought adapted flora were prevalent in the region during the B-A (Bacon et al., 2006; Nowak et al., 2017). Data from our study are broadly consistent with these regional paleoenvironmental data.

5.3. Pleistocene-Holocene transition (Unit III, ~12.8–10.9 cal kyr B.P)

Unit III (~12.8–10.9 cal kyr B.P.) marks an important transition in facies and chemostratigraphy. The lower portion of this unit (655–591 cm; ~12.8–12.0 cal kyr B.P.) captures most of the Younger Dryas (Y-D) stadial. Ali (2018) presented paleo-shoreline data that indicated Mono Lake level abruptly rose to a highstand (~2090 m asl) during the Y-D, potentially responding to atmospheric teleconnections governed by cold sea surface temperatures and sea ice in the North Atlantic (Chiang et al., 2014; Cvijanovic et al., 2017). The Y-D is not particularly well-dated in other sedimentary archives from eastern California and the Great Basin, and the records that exist seem to show some sub-millennial variability through the interval that includes the stadial (Mensing, 2001; Benson et al., 2002; Oviatt et al., 2005; Orme and Orme, 2008; MacDonald et al., 2008). Still others have documented lake transgressions towards the end of the Y-D, for example the Gilbert shoreline in the Bonneville Basin (Oviatt, 2014). Near Unit III's basal contact, TOC and BiSi concentrations rise, whereas MS declines (Fig. 5). Limited terrigenous detritus is consistent with a highstand that migrated delta fronts to the west and limited the influence of turbidity currents. Thus, we interpret that organic facies development during the Y-D highstand was mostly controlled by production and preservation dynamics. $\delta^{13}C_{ORG}$ increases during the Y-D, which is consistent with higher production; $C{:}N_{ATM}$ values (12–15) and amorphous organic matter on smear slides suggest the dominance of algae. The lower Unit III muds are grey-black and finely laminated, which we interpret as reflective of low lake-floor oxygen levels that limited bioturbation. Therefore, high TOC concentrations were likely influenced by higher primary production, as well as a lake-floor environment conducive to preserving organic matter.

Transitioning up section from the Y-D interval, a pronounced shift occurs in Unit III sedimentology, as mud color changes from black to olive and red (Fig. 6). Laminations in the olive and red muds are discontinuous and marked by diffuse contacts. We interpret this transition to mark falling water levels and a change in redox condition on the lake floor that allowed for periodic oxygen ventilation and reworking by benthos beginning after ~12.0 kyr B.P. (Potter et al., 2005). Paleoshoreline data from Ali (2018) suggest that water level elevation fell to < 1980 m asl during this regression. Thin graded sand beds in this interval are interpreted as turbidites, which may have been generated by gravitational instabilities on lowstand delta fronts. Large changes in TOC, BiSi, $\delta^{15}N_{ORG}$ and $C{:}N_{ATM}$ are also apparent during this post Y-D regression (Fig. 5). BiSi data suggest variable but relatively high diatom productivity during this interval, which is consistent with mean $\delta^{13}C_{ORG}$ of −25.0‰. TOC variability likely reflects the interplay between intermittent oxidation on the lake floor and contributions of organic matter from multiple sources. High $C{:}N_{ATM}$ in this interval appears to be most influenced by macrophyte debris, which is prominent on smear slides along with amorphous organic matter. The high $\delta^{15}N_{ORG}$ in this interval could be influenced by a number of processes, including: (a) inputs from ^{15}N-enriched lake margin macrophytes; (b) high productivity spurring depletion of ^{14}N, or (c) a change in the DIN pool, perhaps as lake waters become more concentrated by evaporation during the lowstand (Talbot, 2002). Taken together, we interpret that the geochemical data are most consistent with offshore focusing of nearshore organic matter coupled with relatively high algal production during the regression from ~12.0–10.9 cal kyr B.P. Wave-enhanced resuspension of nearshore organic material is a process that has been invoked to explain high Mono Lake TOC concentrations in the recent past (Tenzer et al., 1997; Meyers and Lallier-Verges, 1999), and the presence of fragmented ostracod valves on smear slides supports this interpretation for late Unit III time. A less likely alternative invokes the influence of falling lake levels on salinity, which may have enhanced organic matter preservation by inhibiting respiration or strengthening water column stratification (Meyers and Teranes, 2002). While this mechanism could explain high $\delta^{15}N_{ORG}$, the diffuse red and olive-green laminated muds strongly argue against water column stratification and lake-floor anoxia.

5.4. Early and Middle Holocene (Units IV and V, ~10.9–8.6 cal kyr B.P. and ~8.6–4.3 cal kyr B.P)

Holocene units recovered in the UWI-MONO15-1C/D are olive and brown laminated muds with occasional grey or black laminae or thin beds (Fig. 7). The change in color for strata above the Unit III Y-D interval is one of the most pronounced transitions in the core. Similar to Pleistocene-aged muds, laminations are the dominant sediment structures in Holocene-aged deposits. Average sediment texture in Holocene units is noticeably finer than the silt and dropstone-rich Pleistocene units, which we interpret as the diminished influence of glacial runoff. Overall, the pace of sedimentation in the Holocene declines about 50% from Pleistocene rates, which suggests that dilution was less important to organic facies development (Fig. 3).

Unit IV (~10.9–8.6 cal kyr B.P.) contains some of the most finely laminated muds in the UWI-MONO15-1C/D core; we interpret these intervals to have had minimal bioturbation of the core site and potentially sedimentation influenced by strong seasonality (Fig. 4). Other Unit IV sections contain blebby laminae or thicker laminations with diffuse contacts (Fig. 7). The diversity in laminae character is most consistent with variable redox conditions on the lake floor. The MS response of Unit IV is generally very low, with the exception of an upward-fining bed of grey fine sand, coarse silt, and mud near the basal contact, which produces a symmetrical MS peak (Fig. 4). Unlike turbidites encountered at older levels, which are coarse, thin, and exhibit relatively abrupt internal textural transitions, this feature is a relatively thick and homogenous with high mud content. Several grey homogenites of varying thickness with lower MS values exist near the base of Unit IV (Fig. 5). The presence of these grey muddy homogenites may have resulted from floods that remobilized similarly colored WCF deposits near the lakeshore; this interpretation is consistent with a seasonally wet paleoclimate. Following this interpretation, sediment-laden flood flows transform into hyperpycnal flows that traveled down slope, ultimately producing a fine-grained turbidite (Osleger et al., 2009). Alternatively, this package may have resulted from remobilization of hemipelagic or prodelta muds during an episode of subaqueous slope

failure (e.g., Moernaut et al., 2014; Ivory et al., 2014), though we consider this possibility less likely due to the color and texture of these features.

Most geochemical indicators shift sharply at the Unit III-IV contact; geochemical changes from ~10.9–8.6 cal kyr B.P. are gradual and suggest a relatively stable paleoenvironment. The decline in $C:N_{ATM}$ is interpreted as a shift in organic provenance that favored lacustrine algae, which is also consistent with $\delta^{13}C_{ORG}$ (Fig. 8). TOC, BiSi, and $\delta^{13}C_{ORG}$ suggest moderate to high productivity in Mono Lake during the early Holocene, but we interpret that preservation dynamics were likewise important. Strata characterized by sharp, ultra-thin laminations provide evidence in support of an anoxic lake floor, and the very fine texture of these muds likely limited oxidants in pore spaces, further enhancing organic matter preservation. This interpretation is supported by the research of Newton (1994), who suggested that starting around ~10 kyr B.P., Mono Lake was meromictic. Meromictic lakes have a well-mixed epilimnion separated by a pycnocline from a deeper hypolimnion. It is not unusual for meromictic lakes to preserve considerable sedimentary organic matter, as low oxygen levels limit bioturbation and respiration (Talbot and Livingstone, 1989; Meyers and Teranes, 2002). However, the absence of water-column turnover renders some meromictic lakes nutrient limited, but geochemical evidence for elevated primary productivity in Unit IV does not support this interpretation. Smear slides from Unit IV contain diatoms and BiSi varies widely, but amorphous organic matter is more abundant, which we interpret as evidence for diverse algae types in the early Holocene at Mono Lake. Relatively low $\delta^{15}N_{ORG}$ suggests the potential for reduced vertical circulation of DIN due to the presence of a chemocline, which may have allowed other algae, potentially including those that fix N_2, to outcompete diatoms. Together, these data point to meromixis as an important control on organic facies at this time.

Low carbonate content in a shallow water core from Mono Lake was interpreted as evidence for a relatively wet paleoclimate in the Early Holocene (Zimmerman et al., in press), and other research supports a cool and wet Early Holocene, which influenced organic facies development by limiting the transport of terrestrial organic matter via prolonged snow cover, restricted plant types, and reduced runoff (Davis, 1999; Noble et al., 2016). Yet other studies, particularly pollen-based vegetation reconstructions of central and southern Sierra Nevada hydroclimate, paint a different, more arid picture for the Early Holocene (Davis et al., 1985; Anderson, 1990; Anderson and Smith, 1994). Less clear, however, are the influences of soil quality and temperature on those high elevation plant communities following deglaciation. Oviatt et al. (2015) likewise noted a dry climate, but with locally wet paleoenvironments due to heavy groundwater seepage from mountain and piedmont aquifers during MIS 2. Mono Lake paleo-shorelines dated to this time period are complex and indicate several low amplitude lake level oscillations between ~1975–1955 m asl (Ali, 2018). These relatively small changes in water level elevation appear to have had minor influence on deepwater facies in the early Holocene, and organic facies development is best explained by moderate to high production from a diverse suite of algae, and lake floor redox conditions that facilitated excellent preservation.

The medium brown muds of Unit V have low MS response, and the most prominent peaks are correlative with three distinct tephra layers that also appear in shallow water deposits (Fig. 2) (Zimmerman et al., in press). The basal sub-unit Va spans ~8.6–6.3 cal kyr B.P., an interval for which paleo-shoreline information is unavailable, but the shallow-water BINGO core contains finely laminated, low-carbonate muds until at least 7 kyr BP (Zimmerman et al., in press). The transition between Unit IV and the overlying Unit Va is marked by a shift to thick laminations with diffuse contacts and the first appearance of coarse-grained laminations in the record. Unit Va time overlaps with the Holocene Hypsithermal, an interval inferred to be relatively dry at Mono Lake based on pollen and carbonate sedimentology (Davis, 1999; Zimmerman et al., in press). Our sedimentological, elemental and stable isotopic data are consistent with declining water levels during Unit Va, but we interpret that the core site likely remained within the profundal zone. The coarse laminae in Unit Va resemble shallow water tufa sands and aragonite "flake mud" described by Newton (1994). Ali (2018) and Lajoie (1968) suggested that algal tufa formed in the photic zone at Mono Lake, which Newton (1991) observed to be ≤6 m deep in the modern lake. Therefore, the presence of tufa grains in Unit Va laminations suggests that: (a) the core site was within the photic zone during deposition, or (b) shallow water sediments were reworked and transported offshore before settling to the lake floor. The majority of our data favor the latter interpretation. For example, coarse laminae are interbedded with bundles of diffuse-boundary muddy laminae, which argues against deposition in the wave-swept, high energy littoral zone. We interpret that $C:N_{ATM}$ and $\delta^{13}C_{ORG}$ values likewise reflect the influence from nearshore, ^{12}C-enriched macrophytes and potentially C_4 plants. Because C_4 plants are adapted to water stress, these data are consistent with a relatively dry climate, and thus low lake level, at Mono Lake and with the watershed vegetation reconstruction of Davis (1999). Notably, early Unit Va occurs near the end of a period of elevated late summer Northern Hemisphere insolation, which may have expanded North American monsoon activity (Barron et al., 2012). It is plausible that periodic summer rainstorms influenced wave action and reworking of Mono Lake's littoral during Unit Va time. By analogy, Godsey et al. (2011) interpreted that storms were important agents for reworking nearshore carbonates into offshore environments during a regressive phase of Lake Bonneville.

Unit Vb (~6.3–4.3 cal kyr B.P.) strata are characterized by light brown, diffuse muddy laminae; coarse laminations are absent, which suggests that offshore transport of nearshore material declined. From a regional perspective, the period of ~6.3–3.0 kyr B.P. is represented in some proxy records from the eastern Sierra region as a relatively wet paleoclimate (Mensing et al., 2004; Noble et al., 2016), whereas other data suggest aridity and continuation of the warm hypsithermal (Benson et al., 2002; Potito et al., 2006; MacDonald et al., 2016). We interpret that organic provenance shifted in Unit Vb relative to Unit Va, with lesser contributions from C_4 vegetation and macrophytes suggested by lower $\delta^{13}C_{ORG}$ (Fig. 8). Mean TOC concentration rises to ~3.0 wt%, but BiSi decreases in this interval. The declining relevance of diatoms suggests paleo-production from a diverse suite of algae. $\delta^{15}N_{ORG}$ declines towards the upper contact, which may imply water column stratification and limited vertical DIN cycling that allowed several algae types to thrive in the lake. We interpret that Mono Lake level likely increased in Unit Vb, driving increased algal production and improved preservation dynamics on the lake floor relative to underlying Unit Va deposits.

6. Conclusions

Data from a new radiocarbon-dated deepwater sediment core, coupled with insights from an existing well-dated paleo-shoreline chronology, were used to assess paleolimnological changes at Mono Lake over the Pleistocene-Holocene transition. Changes in laminae character, sediment composition, color, MS, TOC, BiSi and stable isotopes were used to test the hypothesis that environmental changes control organic facies development in deepwater over millennial time scales. Data produced by this study support the hypothesis. Organic facies in the late Pleistocene developed under the influence of high amplitude changes in water level, a nearby glaciated watershed, and the presence of lake ice. Dilution was especially important to organic facies development during late Pleistocene regressions, driven by riverine incision, deltaic progradation, and the transport of glacial flour and dropstones to the lake; these processes may have influenced paleoproductivity via turbidity. The Y-D was a pronounced lake level highstand at Mono Lake that resulted in moderate to high paleo-production and good organic matter preservation at depth, in evidence from black-grey laminated muds. Falling lake level following the Y-D

resulted in a strong change in lake floor redox conditions, which led to periodic ventilation and reworking by benthos. The geochemical data suggest that macrophyte organic matter was focused offshore by waves at this time, which coupled with relatively high algal production, facilitated the accumulation of organic-rich sediments.

Lower amplitude lake level fluctuations characterized the Holocene paleoenvironment at Mono Lake, and data from the present study suggest moderate to high paleo-production from a diverse suite of algae and preservation-enhancing meromixis were likely for periods inferred to be relatively wet in the Sierra Nevada. The appearance of diverse laminae types, including coarse laminations, appear to capture the transition into the drier Middle Holocene. Organic facies development at this time was strongly influenced by allochthonous organic material mixing with lacustrine algae, likely capturing the influence of wave reworking of low-density macrophyte organic matter offshore. These data shed new light on paleolimnological processes in the eastern Sierra Nevada during the late Quaternary, which are crucial for understanding the evolution of California's headwaters under the influence of global environmental changes.

Supplementary data to this article can be found online at https://doi.org/10.1016/j.palaeo.2019.109565.

Declaration of competing interest

The authors declare that they have no known competing financial interests or personal relationships that could have appeared to influence the work reported in this paper.

Acknowledgements

This research was supported by the US NSF (Award #1829093) and permitted by the Mono/Inyo National Forest. We are grateful to the staff at the National Lacustrine Core Facility for their support and curation of UWI-MONO15-1C/D. Support from S. Hemming, S. Colman, R. Niederreiter, M. Niederreiter, J. Backus, A. Conner, S. Azeem and J. Lucas was greatly appreciated. We are indebted to the Mono Lake Committee, especially B. Miller, for their assistance and enthusiasm. We thank our reviewers for their helpful comments. This is LLNL-JRNL-782377.

References

Ali, G.A.H., 2018. Late Glacial and Deglacial Fluctuations of Mono Lake, California. [Ph.D. thesis]. Columbia University (255 p).
Anderson, R.S., 1990. Holocene forest development and paleoclimates within the central Sierra Nevada, California. The Journal of Ecology 470–489.
Anderson, R.S., Smith, S.J., 1994. Paleoclimatic interpretations of meadow sediment and pollen stratigraphies from California. Geology 22 (8), 723–726.
Bacon, S.N., Burke, R.M., Pezzopane, S.K., Jayko, A.S., 2006. Last glacial maximum and Holocene lake levels of Owens Lake, eastern California, USA. Quat. Sci. Rev. 25, 1264–1282.
Bailey, R.A., Dalrymple, G.B., Lanphere, M.A., 1976. Volcanism, structure, and geochronology of long valley caldera, mono county, california. J. Geophys. Res. 81 (5), 725–744.
Bailey, R.A., 2004. Eruptive History and Chemical Evolution of the Precaldera and Postcaldera Basalt-dacite Sequences, Long Valley, California: Implications for Magma Sources, Current Seismic Unrest, and Future Volcanism (No. 1692). US Department of the Interior, US Geological Survey.
Barron, J.A., Metcalfe, S.E., Addison, J.A., 2012. Response of the North American monsoon to regional changes in ocean surface temperature. Paleooceanography 28, 1–17.
Bennett, M.R., Doyle, P., Mather, A.E., 1996. Dropstones: their origin and significance. Palaeogeogr. Palaeoclimatol. Palaeoecol. 121, 331–339.
Benson, L.V., Lund, S.P., Burdett, J.W., Kashgarian, M., Rose, T.P., Smoot, J.P., Schwartz, M., 1998. Correlation of Late-Pleistocene lake-level oscillations in Mono Lake, California, with North Atlantic climate events. Quat. Res. 49, 1–10.
Benson, L., Kashgarian, M., Rye, R., Lund, S., Paillet, F., 2002. Holocene multidecadal and multicentennial droughts affecting Northern California and Nevada. Quat. Sci. Rev. 21, 659–682.
Benson, L., Linsley, B., Smoot, J., Mensing, S., Lund, S., Stine, S., Sarna-Wojcicki, A., 2003a. Influence of the Pacific Decadal Oscillation on the climate of the Sierra Nevada, California and Nevada. Quat. Res. 59, 151–159.
Benson, L., Lund, S., Negrini, R.M., Linsley, B., Zic, M., 2003b. Response of North American Great Basin Lakes to Dansgaard-Oeschger oscillations. Quat. Sci. Rev. 22, 2239–2251.
Bischoff, J.L., Herbst, D.B., Rosenbauer, R.J., 1991. Gaylussite formation at Mono Lake, California. Geochim. Cosmochim. Acta 55 (6), 1743–1747.
Blaauw, M., Christen, J.A., 2011. Flexible paleoclimate age-depth models using an autoregressive gamma process. Bayesian Anal. 6, 457–474.
Bohacs, K.M., Carroll, A.R., Neal, J.E., Mankiewicz, P.J., 2000. Lake-basin type, source potential, and hydrocarbon character: an integrated sequence-stratigraphic- geochemical framework. In: Gierlowski-Kordesch, E.H., Kelts, K.R. (Eds.), Lake Basins Through Space and Time: AAPG Studies in Geology. 46. pp. 3–34.
Chiang, J.C.H., Lee, S., Putnam, A.E., Wang, X., 2014. South Pacific Split Jet, ITCZ shifts, and atmospheric North-South linkages during abrupt climate changes of the last glacial period. Earth Planet. Sci. Lett. 406, 233–246.
Colman, S.M., Yua, S., Anc, A., Shend, J., Henderson, A.C.G., 2007. Late Cenozoic climate changes in China's western interior: a review of research on Lake Quinghai and comparison with other records. Quat. Sci. Rev. 26, 2281–2300.
Colman, S.M., Hemming, S.R., Stine, S., Zimmerman, S.R.H., 2014. The effects of recent uplift and volcanism on deposition in Mono Lake, California, from seismic-reflection (CHIRP) profiles. Journal of Geophysical Research: Solid Earth 119, 1–16.
Conley, D.J., Schelske, C.L., 2002. Biogenic silica. In: Smol, J.P., Birks, H.J.B., Last, W.M., Bradley, R.S., Alverson, K. (Eds.), Tracking Environmental Change Using Lake Sediments. 3. Kluwer Academic Publishers, Dordrecht, Netherlands, pp. 281–293.
Costa-Cabral, M., Roy, S.B., Maurer, E.P., Mills, W.B., Chen, L., 2013. Snowpack and runoff response to climate change in Owens Valley and Mono Lake watersheds. Clim. Chang. 116 (1), 97–109.
Cvijanovic, I., Santer, B.D., Bonfils, C., Lucas, D.D., Chiang, J.C.H., Zimmerman, S., 2017. Future loss of Arctic sea-ice cover could drive a substantial decrease in California's rainfall. Nat. Commun. 8 (1947), 1–10.
Davis, O.K., 1999. Pollen analysis of a late glacial and Holocene sediment core from Mono Lake, Mono County, California. Quat. Res. 52, 243–249.
Davis, O.K., Anderson, R.S., Fall, P.L., O'Rourke, M.K., Thompson, R.S., 1985. Palynological evidence for early Holocene aridity in the southern Sierra Nevada, California. Quat. Res. 24 (3), 322–332.
Diffenbaugh, N.S., Swain, D.L., Touma, D., 2015. Anthropogenic warming has increased drought risk in California. Proc. Natl. Acad. Sci. 112 (13), 3931–3936.
Ellis, G.S., Katz, B.J., Scholz, C.A., Swart, P.K., 2015. Organic sedimentation in modern lacustrine systems: a case study from Lake Malawi, East Africa. In: Larsen, D., Egenhoff, S.O., Fishman, N.S. (Eds.), Paying Attention to Mudrocks: Priceless!. 515. Geological Society of America Special Paper, pp. 19–47. https://doi.org/10.1130/2015.2515(02).
Forester, R.M., 1987. Late Quaternary paleoclimate records from lacustrine ostracods. In: Ruddiman, W.F., Wright Jr.H.E. (Eds.), North America and Adjacent Ocean During the Last Glaciation. The Geology of North America. Vol. K-3. Geological Society of America, Boulder, CO, pp. 261–276.
Girardclos, S., Schmidt, O.T., Sturm, M., Ariztegui, D., Pugin, A., Anselmetti, F.S., 2007. The 1996 AD delta collapse and large turbidite in Lake Brienz. Mar. Geol. 241, 137–154.
Godsey, H.S., Oviatt, C.G., Miller, D.M., Chan, M.A., 2011. Stratigraphy and chronology of offshore to nearshore deposits associated with the Provo shoreline, Pleistocene Lake Bonneville, Utah. Palaeogeogr. Palaeoclimatol. Palaeoecol. 310, 442–450.
Griffin, D., Anchukaitis, K.J., 2014. How unusual is the 2012–2014 California drought? Geophys. Res. Lett. 41, 9017–9023.
Håkanson, L., 1982. Bottom dynamics in lakes. Hydrobiologica 91, 9–22.
Hayhoe, K., Cayan, D., Field, C.B., Frumhoff, P.C., Maurer, E.P., Miller, N.L., Moser, S.C., Schneider, S.H., Cahill, K.N., Cleland, E.E., Dale, L., Drapek, R., Hanemann, R.M., Kalkstein, L.S., Lenihan, J., Lunch, C.K., Neilson, R.P., Sheridan, S.C., Verville, J.H., 2004. Emissions pathways, climate change, and impacts on California. Proc. Natl. Acad. Sci. 101 (34), 12422–12427.
Herbst, D.B., 1990. Distribution and abundance of the alkali fly (*Ephydra hians*) say at Mono Lake, California (USA) in relation to physical habitat. Hydrobiologia 197 (1), 193–205.
Herbst, D.B., Blinn, D.W., 1998. Experimental mesocosm studies of salinity effects on the benthic algal community of a saline lake. J. Phycol. 34, 772–778.
Hildreth, W., 2004. Volcanological perspectives on Long Valley, Mammoth Mountain, and Mono Craters: several contiguous but discrete systems. J. Volcanol. Geotherm. Res. 136 (3-4), 169–198.
Hodelka, B.N., 2018. Stratigraphy and Organic Geochemistry Reveal Patterns of Late Quaternary Paleo-Productivity at Mono Lake, California. [M.S. thesis]. University of Kentucky, Lexington (93 p).
Hodell, D.A., Schelske, C.L., 1998. Production, sedimentation, and isotopic composition of organic matter in Lake Ontario. Limnol. Oceanogr. 43, 200–214.
Howarth, J.D., Fitzsimons, S.J., Norris, R.J., Jacobsen, G.E., 2012. Lake sediments record cycles of sediment flux driven by large earthquakes on the Alpine fault, New Zealand. Geology 40, 1091–1094.
Ivory, S.J., McGlue, M.M., Ellis, G.S., Lézine, A.M., Cohen, A.S., Vincens, A., 2014. Vegetation controls on weathering intensity during the last deglacial transition in southeast Africa. PLoS One 9 (11), e112855.
Jellison, R., Melack, J., 1993a. Algal Photosynthetic Activity and its Response to Meromixis in Hypersaline Mono Lake. 38(4). American Society of Limnology and Oceanography, California, pp. 818–837.
Jellison, R., Melack, J.M., 1993b. Meromixis in hypersaline Mono Lake, California. 1. Stratification and vertical mixing during the onset, persistence, and breakdown of meromixis. American Society of Limnology and Oceanography 38 (5), 1008–1019.
Jellison, R., Miller, L.G., Melack, J.M., Dana, G.L., 1993. Meromixis in hypersaline Mono Lake, California. 2. Nitrogen fluxes. American Society of Limnology and Oceanography 38 (5), 1020–1039.
Jellison, R., Anderson, R.F., Melack, J.M., Heil, D., 1996. Organic matter accumulation in

sediments of hypersaline Mono Lake during a period of changing salinity. Limnol. Oceanogr. 41 (7), 1539–1544.
Jennings, C.W., Gutierrez, C., Bryant, W., Saucedo, G., Wills, C., 2010. Geologic Map of California. In: California Geological Survey, scale 1:750000.
John, D.A., duBray, E.A., Blakely, R.J., Fleck, R.J., Vikre, P.G., Box, S.E., Moring, B.C., 2012. Miocene magmatism in the Bodie Hills volcanic field, California and Nevada: a long-lived eruptive center in the southern segment of the ancestral Cascades arc. Geosphere 8 (1), 44–97.
Kelleher, P.C., Cameron, K.L., 1990. The Geochemistry of the Mono Craters-Mono Lake Islands Volcanic Complex, eastern California. J. Geophys. Res.: Solid Earth 95 (B11), 17643–17659.
Kociolek, J.P., Herbst, D.B., 1992. Taxonomy and distribution of benthic diatoms from Mono Lake, California, U.S.A. Transactions of the American Microscopial Society 111, 338–355.
Laird, K.R., Fritz, S.C., Grimm, E.C., Mueller, P.G., 1996. Century-scale paleoclimatic reconstruction from Moon Lake, a closed-basin lake in northern Great Plains. Limnol. Oceanogr. 41 (5), 890–902.
Lajoie, K.R., 1968. Quaternary Stratigraphy and Geologic History of Mono Basin, Eastern California. [Ph.D. thesis]. University of California (383 p).
Lowenstein, T.K., Li, J., Brown, C., Roberts, S.M., Ku, T., Luo, S., Yang, W., 1999. 200 k.y. paleoclimate record from Death Valley salt core. Geology 27, 3–6.
MacDonald, G.M., Moser, K.A., Bloom, A.M., Porinchu, D.F., Potito, A.P., Wolfe, B.B., Edwards, T.W.D., Petel, A., Orme, A.R., Orme, A.J., 2008. Evidence of temperature depression and hydrological variations in the eastern Sierra Nevada during the Younger Dryas stade. Quat. Res. 70, 131–140.
MacDonald, G.M., Moser, K.A., Bloom, A.M., Potito, A.P., Porinchu, D.F., Holmquist, J.R., Hughes, J., Kremenetski, K.V., 2016. Prolonged California aridity linked to climate warming and Pacific Sea surface temperature. Sci. Rep. 6, 33325.
MacIntyre, S., Flynn, K.M., Jellison, R., Romero, J.R., 1999. Boundary Mixing and Nutrient Fluxes in Mono Lake, California. 44(3). American Society of Limnology and Oceanography, pp. 512–529.
Marcaida, M., Vazquez, J.A., Stelten, M.E., Miller, J.S., 2019. Constraining the Early Eruptive History of the Mono Craters Rhyolites, California, Based on 238U-230Th Isochron Dating of Their Explosive and Effusive Products. Geochem. Geophys. Geosyst. 20 (3), 1539–1556.
Mauer, E.P., 2007. Uncertainty in hydrologic impacts of climate change in the Sierra Nevada, California, under two emissions scenarios. Clim. Chang. 82, 309–325.
McFadden, M.A., Mullins, H.T., Patterson, W.P., Anderson, W.T., 2004. Paleoproductivity of eastern Lake Ontario over the past 10,000 years. American Society of Limnology and Oceanography 49 (5), 1570–1581.
McGlue, M.M., Ellis, G.S., Cohen, A.S., 2015. Modern muds of Laguna Mar Chiquita (Argentina): particle size and organic matter geochemical trends from a large saline lake in the thick-skinned Andean foreland. In: Geological Society of America Special Paper. 515. pp. 1–8.
McGlue, M.M., Palacios-Fest, M.R., Cusminsky, G.C., Camacho, M., Ivory, S.J., Kowler, A.L., Chakraborty, S., 2017. Ostracode biofacies and shell chemistry reveal Quaternary aquatic transitions in the Pozuelos Basin (Argentina). Palaios 1 (32(6)), 413–428.
Mensing, S.A., 2001. Late-Glacial and Early Holocene vegetation and climate change near Owens Lake, Eastern California. Quaternary Research 55, 57–65.
Mensing, S.A., Benson, L., Kashgarian, M., Lund, S., 2004. A Holocene pollen record of persistent droughts from Pyramid Lake, Nevada, USA. Quat. Res. 62, 29–38.
Meyers, P.A., Lallier-Verges, E., 1999. Lacustrine sedimentary organic matter records of late Quaternary paleoclimates. J. Paleolimnol. 21, 345–372.
Meyers, P.A., Teranes, J.L., 2002. Sediment organic matter. In: Last, W.M., Smol, J.P. (Eds.), Tracking Environmental Change Using Lake Sediments. 2. Kluwer Academic Publishers, Dordrecht, Netherlands, pp. 239–269.
Moernaut, J., Van Daele, M., Heirman, K., Fontijin, K., Strasser, M., Pino, M., Urrutia, R., Batist, M., 2014. Lacustrine turbidites as a tool for quantitative earthquake reconstruction: new evidence for a variable rupture mode in south central Chile. Journal of Geophysical Research: Solid Earth 119. https://doi.org/10.1002/2013JB010738.
Mortlock, R.A., Froelich, P.N., 1989. A simple method for the rapid determination of biogenic opal in pelagic marine sediments. Deep-Sea Res. 36, 1,415–1,426.
Newton, M.S., 1994. Holocene Fluctuations of Mono Lake, California: The Sedimentary Record: Society for Sedimentary Geology Special Publication. 50. pp. 143–157.
Noble, P.J., Ball, G.I., Zimmerman, S.H., Maloney, J., Smith, S.B., Kent, G., Adams, K.D., Karlin, R.E., Driscoll, N., 2016. Holocene paleoclimate history of Fallen Leaf Lake, CA., from geochemistry and sedimentology of well-dated sediment cores. Quat. Sci. Rev. 131, 193–210.
Nowak, R.S., Nowak, C.L., Tausch, R.J., 2017. Vegetation dynamics during last 35,000 years at a cold desert locale: preferential loss of forbs with increased aridity. Ecosphere 8 (7), 1–23.
Orme, A.R., Orme, A.J., 2008. Late Pleistocene shorelines of Owens Lake, California, and their hydroclimatic and tectonic implications. Geol. Soc. Am. Spec. Pap. 439, 207–225.
Osleger, D.A., Heyvaert, A.C., Stoner, J.S., Verosub, K.L., 2009. Lacustrine turbidites as indicators of Holocene storminess and climate: Lake Tahoe, California and Nevada. J. Paleolimnol. https://doi.org/10.1007/s10933-008-9265-8.
Oviatt, C.G., 1997. Lake Bonneville fluctuations and global climate change. Geology 25, 155–158.
Oviatt, C.G., 2014. The Gilbert Episode in the Great Salt Lake Basin, Utah. Utah Geological Survey Miscellaneous Publication, pp. 14-3.
Oviatt, C.G., Miller, D.M., McGeehin, J.P., Zachary, C., Mahan, S., 2005. The younger Dryas phase of great Salt Lake, Utah, USA. Palaeogeogr. Palaeoclimatol. Palaeoecol. 219 (3–4), 263–284.
Oviatt, C.G., Madsen, D.B., Miller, D.M., Thompson, R.S., McGeehin, J.P., 2015. Early Holocene Great Salt Lake, USA. Quat. Res. 84 (1), 57–68.
Potito, A.P., Porinchu, D.F., MacDonald, G.M., Moser, K.A., 2006. A late Quaternary chironomid-inferred temperature record from the Sierra Nevada, California, with connections to northeast Pacific sea surface temperatures. Quat. Res. 66, 356–363.
Potter, P.E., Maynard, J.B., Depetris, P.J., 2005. Mud and Mudstones: Introduction and Overview. Springer, Berlin, Germany (304 p).
Reed, W.E., 1977. Biogeochemistry of Mono Lake, California. Geochim. Cosmochim. Acta 41, 1231–1245.
Reheis, M.C., Stine, S., Sarna-Wojcicki, A.M., 2002. Drainage reversals in Mono Basin during the late Pliocene and Pleistocene. Geol. Soc. Am. Bull. 114 (8), 991–1006.
Rood, D.H., Burbank, D.W., Finkel, R.C., 2011. Chronology of glaciations in the Sierra Nevada, California, from ^{10}Be surface exposure dating. Quat. Sci. Rev. 30 (5–6), 646–661.
Schnurrenberger, D., Russell, J., Kelts, K., 2003. Classification of lacustrine sediments based on sedimentary components. J. Paleolimnol. 29, 141–154.
Shih, P.Y., Lee, J.S., Shinya, R., Kanzaki, N., Pires-daSilva, A., Badroos, J.M., Goetz, E., Sapir, A., Sternberg, P.W., 2019. Newly identified nematodes from Mono Lake exhibit extreme arsenic resistance. Curr. Biol. 29 (19), 3339–3344.
Stine, S., 1987. Mono Lake: The Past 4,000 Years. [Ph.D. thesis]. University of California, Berkeley (859 p).
Stine, S., 1990. Late Holocene fluctuations of Mono Lake, eastern California. Palaeogeogr. Palaeoclimatol. Palaeoecol. 78, 333–381.
Stine, S., 1991. Geomorphic, geographic, and hydrographic basis for resolving the Mono Lake Controversy. Environ. Geol. Water Sci. 17, 67–83.
Sturm, M., Matter, A., 1978. Turbidites and varves in Lake Brienz (Switzerland): deposition of clastic detritus by density currents. In: Modern and Ancient Lake Sediments, pp. 147–168.
Talbot, M.R., 2002. Nitrogen isotopes in palaeolimnology. In: Last, W.M., Smol, J.P. (Eds.), Tracking Environmental Change Using Lake Sediments. 2. Kluwer Academic Publishers, Dordrecht, Netherlands, pp. 401–439.
Talbot, M.R., Johannessen, T., 1992. A high resolution palaeoclimatic record for the last 27,500 years in tropical West Africa from the carbon and nitrogen isotopic composition of lacustrine organic matter. Earth Planet. Sci. Lett. 110, 23–37.
Talbot, M.R., Livingstone, D.A., 1989. Hydrogen index and carbon isotopes of lacustrine organic matter as lake level indicators. Palaeogeogr. Palaeoclimatol. Palaeoecol. 70, 121–137.
Tenzer, G.B., Meyers, P.A., Knoop, P., 1997. Sources and distribution of organic and carbonate carbon in surface sediments of Pyramid Lake, Nevada. J. Sediment. Res. 67, 884–890.
Tunno I., Zimmerman S.H., Brown T.A., Hassel C.A. An improved method for extracting, sorting and AMS dating pollen concentrates from lake sediment. To be submitted to Frontiers in Ecology and evolution, Paleoecology.
Vazquez, J.A., Lidzbarski, M.I., 2012. High-resolution tephrochronology of the Wilson Creek Formation (Mono Lake, California) and Laschamp event using ^{238}U-^{230}Th SIMS dating of accessory mineral rims. Earth Planet. Sci. Lett. 357, 54–67.
Viers, J.H., Rheinheimer, D.E., 2011. Freshwater conservation options for a changing climate in California's Sierra Nevada. In: Marine and Freshwater Research. 63. pp. 266–278.
Weaver, A.J., Saenko, O.A., Clark, P.U., Mitrovica, J.X., 2003. Meltwater Pulse 1A form Antarctica as a trigger of the Bolling-Allerod warm interval. Science 299, 1709–1713.
Wiens, J.A., Patten, D.T., Botkin, D.B., 1993. Assessing ecological impact assessment: Lessons from Mono Lake, California. Ecol. Appl. 3, 595–609.
Zimmerman, S.H., Hemming, S.R., Kent, D.V., Searle, S.Y., 2006. Revised chronology for late Pleistocene Mono Lake sediments based on paleointensity correlation to the global reference curve. Earth Planet. Sci. Lett. 252, 94–106.
Zimmerman, S.R., Brown, T.A., Hassel, C., Heck, J., 2019. Testing Pollen Sorted by Flow Cytometry as the Basis for High-Resolution Lacustrine Chronologies. Radiocarbon 61 (1), 359–374.
Zimmerman, S.R.H., Hemming, S.R., Hemming, N.G., Tomascak, P.B., Pearl, C., 2011a. High-resolution chemostratigraphic record of late Pleistocene lake-level variability, Mono Lake, California. Geological Society of America Bulletin 123, 2320–2334.
Zimmerman, S.H., Pearl, C., Hemming, S.R., Tamulonis, K., Hemming, N.G., Searle, S.Y., 2011b. Freshwater control of ice-rafted debris in the last glacial period at Mono Lake, California, USA. Quat. Res. 76, 264–271.
Zimmerman, S.H., Hemming, S., and Starratt, S., in press. Holocene Sedimentary Architecture and Paleoclimate Variability at Mono Lake, CA. GSA Special Paper 536, From Saline to Freshwater: The Diversity of Western Lakes in Space and Time; Starratt, S.W. and Rosen, M. R., eds. (in rev)